Reconfigurable Force-Balanced Aerial Manipulator for Variable Payload Tasks

MSc Thesis Report

Michele Bianconi

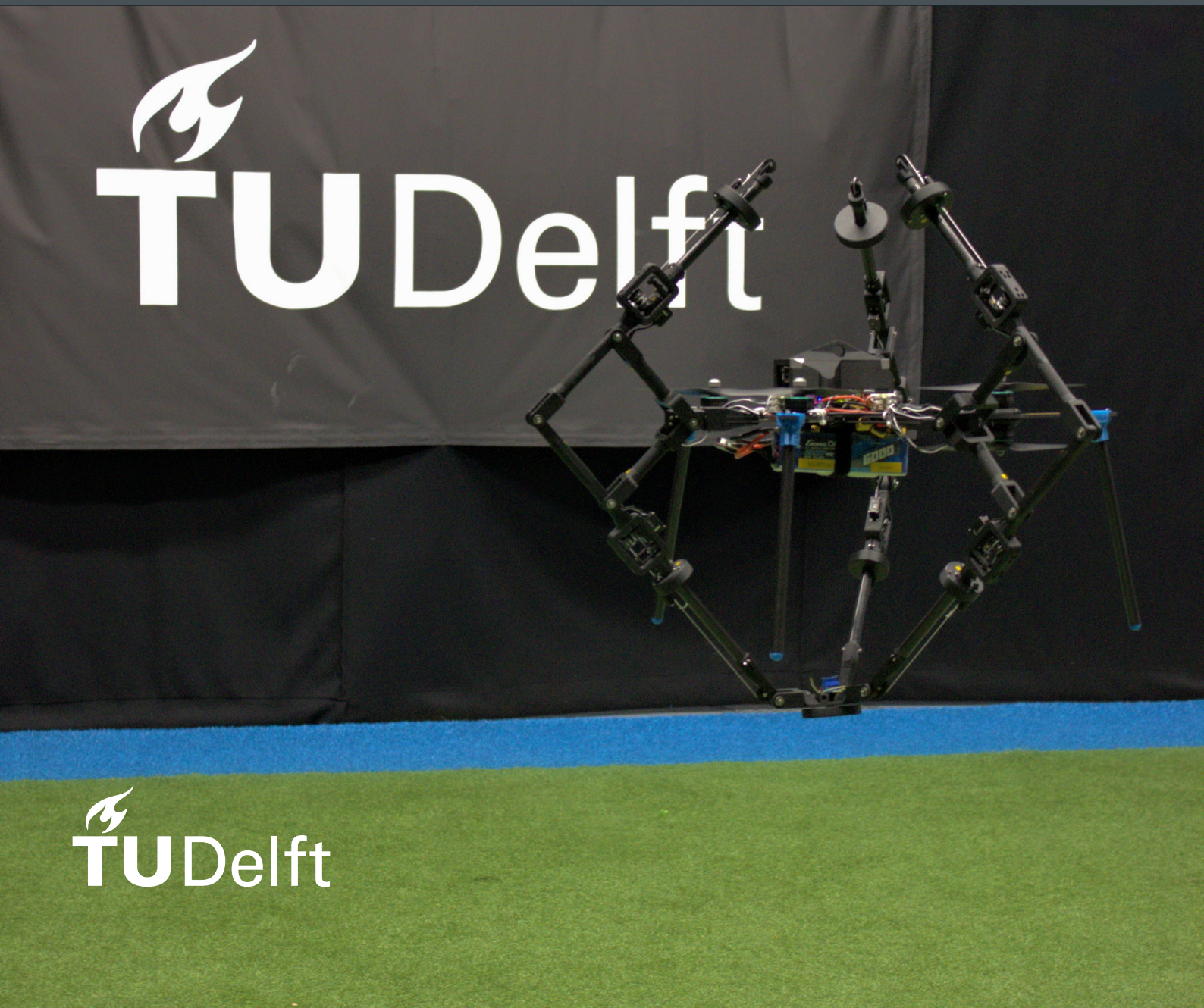

[This page is intentionally left blank]

Reconfigurable Force-Balanced Aerial Manipulator for Variable Payload Tasks

MSc Thesis Report

by

Michele Bianconi

to obtain the degree of Master of Science
at the Delft University of Technology
to be defended publicly on December 4, 2024 at 14:30

Thesis committee:

Chair:	Dr. E. Smeur
Supervisors:	Dr. S. Hamaza
	M. Brummelhuis
External examiner:	Dr. C. Varriale
Place:	Faculty of Aerospace Engineering, Delft
Project Duration:	September, 2023 - November, 2024
Student number:	4857771

An electronic version of this thesis is available at `http://repository.tudelft.nl/`.

Faculty of Aerospace Engineering · Delft University of Technology

Preface

The following report is the culmination of all the work I performed during my master thesis to obtain my Master Degree in Control & Simulation at the Faculty of Aerospace Engineering at Delft University of Technology. The goal of the following work was to showcase that a clever mechanical design for a robotic manipulator, integrated on a drone, can be just as effective compared to other aerial manipulator design approaches. This work specifically focused on using a force-balanced manipulator. Although the original plan was to simply integrate such a manipulator on a drone, I challenged myself to make it reconfigurable for pick-and-place tasks. Hence, I set out to design, build, and test a reconfigurable force-balanced aerial manipulator for variable payload tasks.

This project has been challenging but it allowed me to learn many skills along the way. Although I had built hobby drones in the past this was the first time I designed the entire system from the ground up and really delved deeper in the field of robotics, which I fell in love with throughout the process. I want to thank my supervisor, prof. Salua Hamaza, for the opportunity to work on such an amazing project and also for all the support along the way. Working together I gained a lot of knowledge which I will carry with me to my next chapter. I would also like to thank Martijn for stepping up to be my coach during Salua's maternity leave. I appreciate all your help through to the very end.

I am really glad to have been able to work in the MAVLAB where I had the chance to meet incredible people who have helped me along this journey. A special thank you to Alessandro for helping me with the servos and more. At the MAVLAB I also met Georg, Giorgia, Mahima, and Nils whose friendship I hold close to my heart.

I would like to thank everyone who supported me in my journey. To Hani, thank you for answering all the early aerial manipulator-related questions I bombarded you with and for your friendship. To Antonio, Gigi, Johan, Leo, Loreto, Micha, Sara, and Sofia, thank you for all the fun times we shared over the past years. To Matteo, but also Gigi, Micha, and Nils, thank you for helping me blow off steam on the tennis court. To Alex and Florian for all the fun boy's nights. To Alejandro, thank you for sharing this 6-year adventure with me. To Andre, Ceccio, Fix, and Laffo, my friends back in Italy, grazie per la vostra amicizia. Sono sempre felice di tornare a casa e rivedervi. To Matteo, Alice, and Simone, grazie per essermi stato sempre vicino.

To Rita, my partner in crime, thank you for always listening to me ramble on about my design ideas and plans. Thank you for all your PX4 and writing help, without it so many steps would have taken me twice as long. You made this journey so much more enjoyable and I'm so thankful to have you by my side. Obrigado por tudo.

I also want to thank my family back home for their love and support from afar. To nonna Vanna who supplied me with her ragù and tomato sauce which kept fueled, to nonno Carlo who has always been an inspiration to me. Finally I want to dedicate this work to my parents Virna and Alessandro. You have always supported me throughout life and have always been there for me during the highs and lows. I will always be thankful to have you in my corner, and I hope you know this achievement wouldn't have been possible without you; vi voglio tanto bene, grazie di tutto.

Contents

Part I

Introduction

[This page is intentionally left blank]

Introduction

In the field of robotics, robotic manipulation refers to how robots interact with objects in the environment. Robotic manipulators have been used in production lines since the 1960s to assist with tasks such as handling heavy loads or harmful substances[1]. Over time, these manipulators have evolved to work alongside humans. However, one key limitation of these systems is that their reach is constrained by their physical size.

In recent years, mobile robotic manipulators, robotic arms mounted on mobile platforms, have been developed to overcome this limitation. By enabling robots to move within their environment, these systems dramatically extend their effective reach. Current applications include marine exploration[2] and bomb disposal[3], and ongoing developments aim to integrate such systems into manufacturing and logistics industries for more flexible and cost effective solutions[4].

The emergence of Unmanned Aerial Vehicles (UAVs), or drones, has further spurred the development of aerial manipulators. These are mobile robotic manipulators which use a drone morphology such as a quadrotor as their mobile platform. However using flying robots as mobile platforms presents additional challenges preventing traditional robotic manipulators to be directly integrated on aerial platforms.

The autonomy of drones is limited by their weight thus heavy robotic manipulator are not suitable. Furthermore, compared to static manipulators or ground-based mobile manipulators aerial manipulators are more affected by any reaction generated by the movement of the robotic manipulator. Traditional approaches to addressing these challenges involve designing lightweight manipulators that minimize the produced reaction forces[5]. While effective for some applications, this strategy fails when fast manipulator movements or handling heavy payloads are required.

This research proposes a novel manipulator design that eliminates the reaction forces transmitted to the aerial platform. Instead of relying solely on lightweight systems, this work focuses on creating an inherently reactionless mechanical design. The manipulator is to be integrated on a drone with the ultimate objective of enabling the system to perform variable payload tasks, such as pick-and-place tasks. The rest of this report addresses the central research question:

How can we exploit a reconfigurable mechanical design/morphology to minimize the dynamic coupling between the drone and the manipulator during fast variable payload tasks, such as pick and place?

The report is divided into two parts. First Part II presents the scientific article, detailing the development of the aerial manipulator and its subsystems, as well as the extensive testing performed to validate the system. Then, Part III presents the literature study, conducted before the thesis work, exploring the field of aerial manipulation and summarizing various mechanical and control approaches to aerial manipulator design. This section provides further insight into the decisions made throughout the thesis.

[This page is intentionally left blank]

Part II

Scientific Article

[This page is intentionally left blank]

Reconfigurable Force-Balanced Aerial Manipulator for Variable Payload Tasks

Michele Bianconi
Department of Control & Operations,
Section of Control & Simulation,
BioMorphic Intelligence Lab
Delft University of Technology, The Netherlands

***Abstract*—This research proposes a novel reconfigurable and force-balanced aerial manipulator design for fast variable payload tasks. Its force-balancing properties allow for fast end-effector movements while minimizing disturbances introduced to the aerial platform. The manipulator is composed of three pantograph legs connecting the end-effector to the drone base. Each pantograph is equipped with two moving counter-masses that provide the balancing properties to the manipulator. The counter masses are moved by fast linear actuators allowing the manipulator to be force-balanced for different payloads. Extensive testing, performing end-effector trajectory tracking tasks, was performed both on a floating base setup and in flight. The results indicate that the manipulator significantly decreased the reaction forces transmitted to the base. Specifically, it achieved a 45% reduction when comparing the unbalanced and balanced configurations, and a 17% reduction when these configurations included a 53 [g] payload. The drone's position-tracking error during flight also improved, with reductions of 19% and 34% for the same two configurations, respectively.**

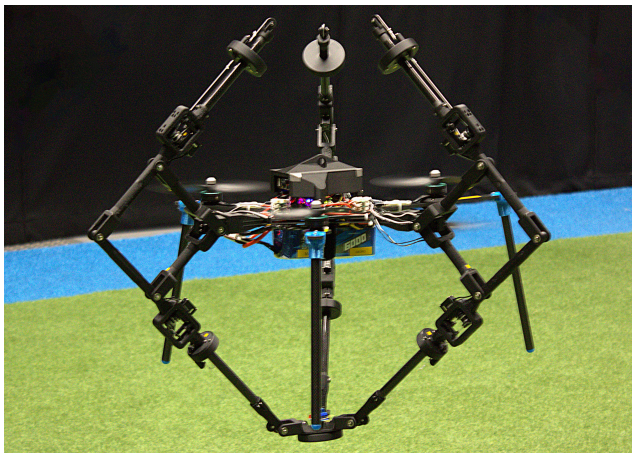

Fig. 1: Picture during flight of reconfigurable force-balanced aerial manipulator.

I. Introduction

The field of aerial manipulation has drawn considerable attention in recent years. This field explores the use of robotic manipulators onboard aerial platforms, such as drones, to perform useful tasks. By adding a manipulator on a moving platform the reachable workspace drastically increases in size, almost only limited by the flight time of the aerial platform.

These systems have various applications including sensor placement[1], contact inspection[2], maintenance for aerial repair[3], construction via aerial screwing[4], and load delivery[5].

Although many advances have been achieved in this field some fundamental problems and tradeoffs persist, such as the integrated control of the robotic manipulator with the aerial platform. Combining a robotic manipulator with a drone couples their dynamics, so any reaction force or moment produced by one affects the other. If the reaction forces or moments generated by the manipulator's movement are too large this could cause the aerial platform to become destabilized.

To tackle this issue complex controllers which account for the coupling between the aerial platform and manipulator have been devised[6]. These however require the complete dynamic model for the entire system which is often more demanding to derive. This approach which considers the manipulator and the drone as one system is called centralized control.

Furthermore, sophisticated aerial platforms coupled with complex control schemes are developed which are more effective at counteracting disturbances produced by the manipulator and its interaction with the environment. An example is the use of fully-actuated platforms such as in the work of Ding et al.[7].

Another approach is to consider the manipulator and the aerial platform as two separate entities. This approach is called decentralized control. In this case, the aerial platform treats the reaction forces and moments produced by the manipulator as unknown disturbances. For the drone to be able to counteract these disturbances they must not be too large. This requires the manipulator to be as lightweight as possible[8].

This approach is faster for development as complex dynamic models are not required but it is still limited by the speed of the motion. A limit is reached when the manipulator movement is too fast such that the reaction forces and moments are no longer negligible and the aerial platform is unable to reject them leading to control loss.

Another alternative which has not been significantly developed in this field is to improve the mechanical design of the manipulator to eliminate the coupling dynamics between the two systems. Kartik et al. proposed a manipulator design for aerial platforms which produces no reaction forces on the

drone. However, this design is balanced only for a specific configuration of the manipulator, so it would not be suitable for varying payload applications such as pick-and-place tasks.

We propose an aerial manipulator design which is force-balanced and capable of reconfiguring itself for different payloads. The main contributions of this work are the following:

- Development of a novel reconfigurable force-balanced manipulator for fast variable payload tasks, along with a lightweight, compact, and fast linear actuator for counter-mass movement.
- Development of a novel drone morphology for synergetic integration with the proposed reconfigurable manipulator.
- Comprehensive experimental validation of the system's motion and flight performance.

II. Related Work

Different designs for aerial manipulator systems have been proposed to limit the coupling effects between the manipulator and the aerial platform. Hamaza et al. incorporated a moving counter mass on a four-bar linkage manipulator to counteract the moment arm generated by the end-effector [9]. This moment balancing reduces strain on the quadrotor by eliminating the need for the quadrotor to compensate for the manipulator's extended moment arm.

In addition to moment balancing, there are three types of balancing: dynamic, force, and static. Dynamic balancing ensures that the reaction forces and moments from manipulator movement are zero. Force balancing occurs when only the net reaction forces on the system's base are zero. Static balancing enables the system to counteract gravitational forces, maintaining stability in any configuration resulting in zero potential energy.

Balancing of manipulators has been an explored field of research, however, the number of these systems that have been physically implemented is limited especially for aerial manipulation applications. [10] presented a dual-arm aerial manipulator with a center of gravity (COG) balancing mechanism. [11] showcased a moving counter mass mechanism with COG balancing properties for a serial manipulator. [12] developed a balanced pantograph gripper for aerial pick-and-place tasks.

There has been theoretical progress in developing balanced parallel manipulators, but few practical implementations have been presented. [13] introduced the force-balancing conditions for Clavel's Delta robot. [14] developed dynamically balanced multi-degrees of freedom mechanisms through the use of a balanced parallel-piped mechanism. [15] presented a family of force-balanced parallel manipulators.

Despite their benefits, there have been limited practical implementations of such balanced parallel manipulators in the field of aerial manipulation. The aforementioned work by Kartik et al.[16] developed a force-balanced parallel manipulator aimed for integration with an aerial platform. Clark et al.[17] implemented a balanced delta-like manipulator design on an aerial platform. This last work achieved good force-balancing properties. However, limitations in the mechanical design, particularly the lack of integration between the manipulator and drone platform, prevented any significant improvement in the drone's tracking performance.

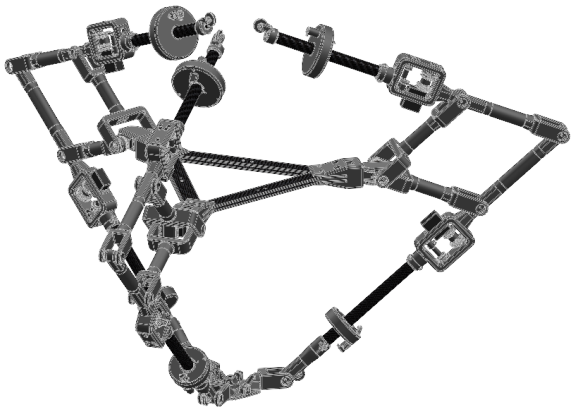

Fig. 2: Render of the reconfigurable force balanced manipulator. The manipulator consists of three pantograph legs. The pantograph's lower portion connects to the end-effector, resulting in a three-degrees-of-freedom parallel manipulator.

Finally, an aspect in which all these balanced configurations are lacking is that they are not balanced for varying payload applications, making them unsuitable for interaction tasks such as pick-and-place tasks. To overcome this limitation de Jong et al.[18] proposed three reconfiguration strategies to adapt the balancing behaviour for varying payload conditions, namely, changing the position of the counter masses, changing the joint locations, or altering the weight of the counter masses.

III. Force-balanced Aerial Manipulator

Force-balanced manipulators are advantageous for aerial systems due to their ability to reduce reaction forces on the drone base caused by manipulator movements. This is particularly beneficial for quadrotors, which cannot directly generate forces to counteract these disturbances. The following section describes the design, fabrication, and control of a reconfigurable, force-balanced aerial manipulator for variable payload tasks. The design strategy focused on treating the manipulator and aerial platform as a cohesive system, ensuring compatibility between the two.

A. Kinematics

The manipulator morphology builds upon the work of Kartik et al. [16] and consists of a fixed base and a moving platform as the end-effector. Three parallel kinematic chains connect the two, forming a three-degree-of-freedom parallel manipulator. Each leg is a pantograph, as shown in Figure 2, of which only the lower portion defines the kinematics and motion of the end-effector.

Figure 3 shows the kinematic parameters of the lower portion of one pantograph (SP_1Q_1). The center of the the fixed base is represented by O and P represents the center of the moving base. At the origin O the Cartesian coordinate frame XYZ is defined. For each pantograph, a coordinate system

$X_{0i}Y_{0i}Z_{0i}$ is defined where $i = 1, 2, 3$ is the pantograph leg number. This coordinate system shares the same XY plane but is rotated by angle θ_i where the X-axis (X_{0i}) points towards the attachment point of pantograph i. The size of the base and end-effector are defined by r_A and r_B which are respectively their radii. To solve the forward kinematics, the transformation from point O to point P is derived link-by-link using the Denavit-Hartenberg convention. Starting from origin O the first joint is a passive revolute joint which rotates the leg around the X_{0i} axis by the angle ϕ_{3i}. The next joint is the active joint which rotates the first link L_1 by the angle ϕ_{1i} with respect to the base. The angle between the first link L_1 and the second link L_2 is denoted by ϕ_{2i}. As the fixed base and moving base are constrained to remain parallel to each other, the next joint after link L_2 is equal to $\phi_{1i}+\phi_{2i}$. Finally, the last joint is equal but opposite in direction to the first passive joint ϕ_{3i}. With these geometric definitions, the Denavit-Hartenberg transformations are defined and the transformation matrix from origin O to point P for one leg of the manipulator is shown below.

$$T_{r_p} = T_{r_Z} T_{t_{ra}} T_{r_{xo}} T_{r_{yo}} T_{t_{L1}} T_{r_{y1}} T_{t_{L2}} T_{r_{y2}} T_{r_{x2}} T_{t_{rb}} T_{r_{Z2}} \quad (1)$$

From this matrix the equations describing the end-effector position as a function of the joints and geometric properties of the manipulator are extracted and reported below.

$$\begin{aligned}
x_{EE} &= \mathrm{r_A} C\Theta_\mathrm{i} - \mathrm{r_B} C\Theta_\mathrm{i} + L_1 C\phi_{11} C\Theta_\mathrm{i} \\
&\quad + L_2 C\phi_{11} C\phi_{21} C\Theta_\mathrm{i} - L_2 C\Theta_\mathrm{i} S\phi_{11} S\phi_{21} \\
&\quad - L_1 S\phi_{11} S\phi_{31} S\Theta_\mathrm{i} - L_2 C\phi_{11} S\phi_{21} S\phi_{31} S\Theta_\mathrm{i} \\
&\quad - L_2 C\phi_{21} S\phi_{11} S\phi_{31} S\Theta_\mathrm{i} \\
y_{EE} &= \mathrm{r_A} S\Theta_\mathrm{i} - \mathrm{r_B} S\Theta_\mathrm{i} + L_1 C\phi_{11} S\Theta_\mathrm{i} \\
&\quad + L_2 C\phi_{11} C\phi_{21} S\Theta_\mathrm{i} + L_1 C\Theta_\mathrm{i} S\phi_{11} S\phi_{31} \\
&\quad - L_2 S\phi_{11} S\phi_{21} S\Theta_\mathrm{i} + L_2 C\phi_{11} C\Theta_\mathrm{i} S\phi_{21} S\phi_{31} \\
&\quad + L_2 C\phi_{21} C\Theta_\mathrm{i} S\phi_{11} S\phi_{31} \\
z_{EE} &= C\phi_{31} L_2 S\phi_{11} + \phi_{21} + L_1 S\phi_{11}
\end{aligned} \quad (2)$$

Where $S()$ and $C()$ denote the sin and cos functions respectively.

Unlike other parallel manipulators[19][20] since the active joint comes after a passive joint the inverse kinematics cannot be solved analytically[16]. Hence, to find a solution for the end-effector position with respect to the active joints geometrical reductions are necessary. First, it can be seen that the length of vector S_1P is not dependent on ϕ_{3i}, therefore by squaring and adding x_{EE}, y_{EE}, z_{EE} we obtain an equation for the passive joint $\phi_2 i$ as a function of ϕ_{1i}. By substituting this equation in the equation for z_{EE} we obtain a relation between the passive joint ϕ_{3i} and the active joint ϕ_{1i}. Finally by replacing the relations between the passive joints and the active joint in the original set of equations for x_{EE}, y_{EE}, z_{EE}, an equation between the desired end-effector positions and the active joint ϕ_{1i} is found.

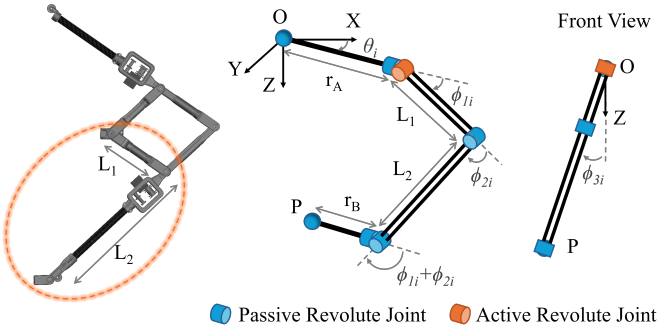

Fig. 3: Schematic diagram of the lower portion of one of the pantograph legs which make up the parallel manipulator. Geometric definitions for the links and joints in the diagram are used to formulate the kinematic model of the manipulator.

Although this can be numerically solved it was found that as the relation is highly non-linear numerical solvers struggle to find the correct solution even for various initial conditions. A different approach was used to numerically solve this problem. From a starting solution space of ϕ_{1i} angles, the passive joints are iteratively solved from the relations previously described. Since $\phi_{3i} = \arccos f\left(\phi_{1i}, x_{EE}, y_{EE}, z_{EE}\right)$ for each ϕ_{1i}, two sets of solutions exist:(ϕ_{1i},ϕ_{2i},ϕ_{3i}) and (ϕ_{1i},ϕ_{2i},$-\phi_{3i}$). The joint angles are checked to be within the joint limits of the manipulator and the end-effector position is computed (x_{EE}, y_{EE}, z_{EE}). If the computed position corresponds to the desired end-effector position the solution is found.

B. Workspace analysis

To determine the dimensions of the manipulator a sensitivity analysis on the workspace was performed by studying the effect of varying the geometric parameters r_A, r_B, L_1 and L_2. The workspace is found by solving the inverse kinematics iteratively for various locations in the positive XZ quadrant. This leads to an outline of the reachable workspace. The total workspace corresponds to this outline revolved around the Z axis.

A smart search is used to find this outline efficiently. First, the vertical bounds are found by solving the inverse kinematics close to the Z-axis line. A search space between the top and bottom z limit is created. From the top limit, the algorithm searches outwards on the x-axis until the kinematics return no solution. From this point, the search moves to the next z position in the search space. If the kinematics are solved for this location the search moves outwards (positive x direction). If no solution is found for the location the search moves inwards (negative x direction). This process continues for the entire search space.

To compare the workspace across different manipulator configurations, two metrics are used: (1) the maximum area of a rectangle that fits within the workspace, representing the overall workspace size, and (2) the maximum width of

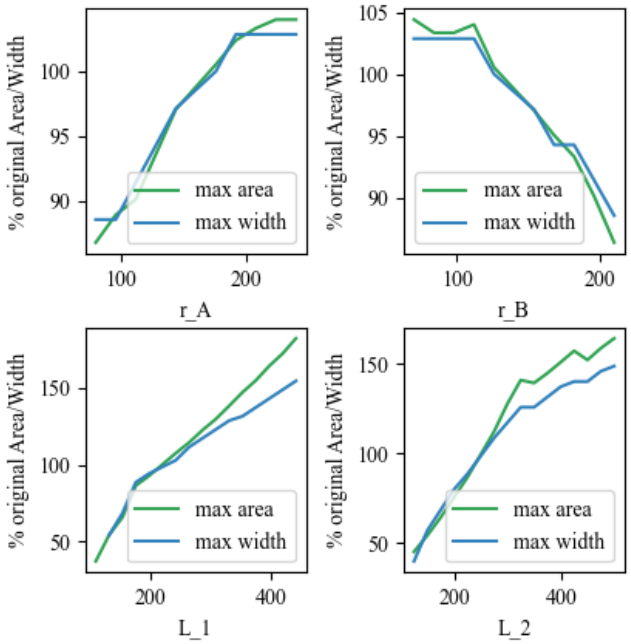

Fig. 4: Results for sensitivity analysis show the effect of varying manipulator parameters r_A, r_B, L_1, and L_2 on workspace characteristics. The maximum area represents the largest rectangle fitting within the workspace outline, while the maximum width represents the widest rectangle at least 10 mm high that fits within this outline. Both metrics increase with r_A, L_1, and L_2, but decrease with r_B.

a 10 mm-high rectangle that fits within the workspace. The latter metric is particularly relevant because the manipulator's workspace should prioritize width over height. While the aerial platform can easily adjust its vertical position, lateral movements require roll or pitch adjustments, which are undesirable for a parallel manipulator with only translational degrees of freedom.

The workspace was computed for an initial manipulator configuration with the following parameters: $r_A = 160mm$, $r_B = 140mm$, $L_1 = 220mm$, and $L_2 = 250mm$. Each parameter was individually varied: r_A and r_B between 0.5 and 1.5 times their initial value, and L_1 and L_2 between 0.5 and 2.0 times their initial values. The sensitivity analysis results are shown in Figure 4.

This figure shows that increasing r_A more than 180 mm or decreasing r_B more than 120 mm provides no additional benefit. Conversely, increasing L_1 and L_2 improves both metrics, with the maximum area metric benefiting more than the maximum width. Based on this analysis, r_A and r_b were set to 180 mm and 65 mm, respectively. The base platform (r_A) was maximized to accommodate the drone's electronics, while the end-effector base (r_B) was minimized to reduce weight, improving the pantograph design's force balancing properties, as discussed in subsection III-C. The dimensions for L_1 and L_2 will be determined in the next section.

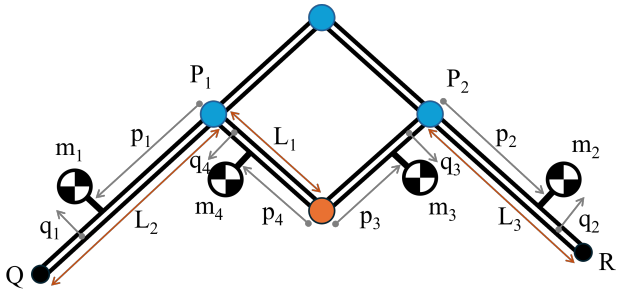

Fig. 5: Schematic diagram defining the mass properties of the force-balanced pantograph mechanism

C. Force-balancing optimization

Our manipulator configuration achieves force-balancing by taking 2D planar force-balanced elements and combining them to create a 3D mechanism. In this case, the planar force-balanced elements are the pantographs, which make up the three legs of the manipulator. Hence, by ensuring each pantograph is force-balanced the resulting manipulator is also force-balanced. The force balancing conditions of the pantograph mechanism were formulated by Van der Wijk [21] and are reported below. Figure 5 shows the dimensions describing the pantograph mechanism.

$$\begin{aligned} m_1 p_1 &= m_2 a_1 + m_3 p_3 \\ m_1 q_1 &= m_3 q_3 \\ m_2 p_2 &= m_1 a_2 + m_4 p_4 \\ m_2 q_2 &= m_4 q_4 \end{aligned} \tag{3}$$

From the pantograph design, we assume that the the center of mass (COM) of the links lies on the axis of the links which leads to $q_1, q_2, q_3, q_4 = 0$. This reduces the system of equations to the following two equations.

$$\begin{aligned} m_1 p_1 &= m_2 a_1 + m_3 p_3 \\ m_2 p_2 &= m_1 a_2 + m_4 p_4 \end{aligned} \tag{4}$$

For the entire manipulator to be force-balanced the mass value m_1 encompasses the mass of the end-effector, hence for each pantograph a third of the weight of the end-effector is counted in the m_1 term. This is then balanced by introducing a counter mass on the opposite side of the pantograph. It can be seen that given fixed dimensions for p_1 and p_2 the pantograph is balanced only for one configuration of the manipulator. Hence, if the mass at the end-effector changes, for example during a pick-and-place task or if the end-effector is replaced the manipulator would not remain force-balanced. To make this manipulator reconfigurable to mass changes at the end-effector, moving counter masses can be placed on the P_1Q and P_2Q links.

The $m_1 p_1$ and $m_2 p_2$ terms can be split in two, namely $\hat{m}_i \hat{p}_i$ and $m_{i\text{CM}} p_{i\text{CM}}$ where $i = 1, 2$ and $m_i p_i = \hat{m}_i \hat{p}_i + m_{i\text{CM}} p_{i\text{CM}}$. The first term encompasses the mass and COM position for all fixed components of link i and the second corresponds to

the mass and COM position of counter mass i. Furthermore, the m_2 term can also be split such that $m_2 = \hat{m_2} + m_\text{p}$ where $\hat{m_2}$ is one-third of the mass of the end-effector structure and m_p is the mass change equal to the payload picked up by the end-effector. p_p is the location of the payload mass which is assumed to be equal to the link length L_2. With these modifications, the force-balancing equations can be rewritten to find the relation between the counter mass locations $p_{1\text{CM}}$, $p_{2\text{CM}}$ and the payload mass m_p.

$$
\begin{aligned}
p_{1\text{CM}} &= -\frac{p_\text{p}}{3m_{1\text{CM}}} \cdot m_\text{p} + \frac{m_2 a_1 + m_3 p_3 - \hat{m_1}\hat{p_1}}{m_{1\text{CM}}} \\
p_{2\text{CM}} &= -\frac{a_2}{3m_{2\text{CM}}} \cdot m_\text{p} + \frac{(\hat{m_1} + m_{1\text{CM}})\, a_2 + m_4 p_4 - \hat{m_2}\hat{p_2}}{m_{2\text{CM}}}
\end{aligned}
\tag{5}
$$

To determine the required mass of the two counter masses an iterative search is performed such that the pantograph remains force-balanced for both a minimum payload of 0 [g] (no payload) and a desired max payload of 60 [g]. A mass of 60 [g] was chosen, as it increases the end-effector mass by 66%, which was deemed sufficient to observe a measurable effect during testing. With these limits on the payload the required limits for the counter mass positions $p_{1\text{CM}}$, $p_{2\text{CM}}$ are determined. The lightest sum of $m_{1\text{CM}}$ and $m_{2\text{CM}}$ which satisfies the geometric limits of the pantograph is the solution for the counter mass weights.

To determine the dimensions of links L_1 and L_2 an optimization based on the force balancing relations was performed. These links correspond to the dimensions $a_1 = a_2$ and P_1Q in Figure 5. From an original prototype of the pantograph the mass and COM positions of all joint components were determined. The mass properties for all the links with dimensions a_1, a_2, P_1Q, and P_2R were all determined as a function of their dimension. From this, the force-balanced configuration of the pantograph can be determined as a function of L_1, L_2, L_3 (corresponding to link P_2R), and $3\hat{m_2}$ (corresponding to 3 times the end-effector structure mass). The goal of the optimization is to minimize the total manipulator weight which accounts for the joints, links and counter masses weight.

The optimization variables were fixed between the following limits. L_1 and L_3 were varied between 100 [mm] and 160 [mm]. L_2 was varied between 280 [mm] and 330 [mm]. $3\hat{m_2}$ was varied between 90 [g] and 150 [g]. The optimization was run for these constraints and yielded the following final dimensions: $L_1 = 130$ [mm], $L_2 = 310$ [mm], $L_3 = 160$ [mm], and $3\hat{m_2} = 90$ [g]

From the optimization it was noticed that a local optimum exists for L_1 and L_2, however maximizing L_3 and minimizing the mass of the end-effector yield lighter manipulator configurations. For this reason, the end-effector structure was designed to minimize its mass resulting in a final value of 90.27 [g]. Furthermore, L_3 was limited to a maximum value of 160 [mm] as this was found to be a suitable value for which the top end of the pantograph does not interfere with the body of the aerial platform.

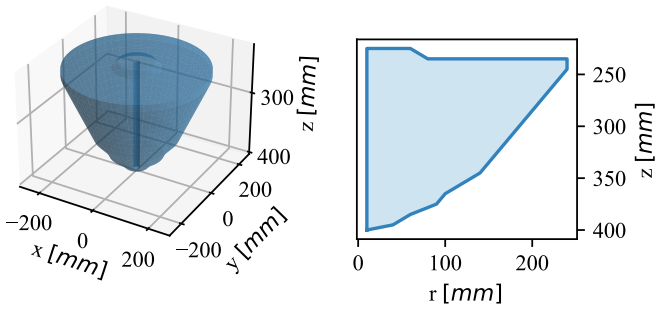

Fig. 6: 3D workspace plot (left) and workspace outline (right) of the final manipulator design.

With all the dimensions defined the workspace of the final manipulator was calculated and is shown in Figure 6.

D. Fast linear actuator design

The counterweights require a mechanism to move them into the desired balancing positions, as outlined in subsection III-C. This necessitates a fast, lightweight linear actuator to minimize reconfiguration time and avoid adding excess weight to links L_2 and L_3, which would reduce the counterweight's effectiveness. Additionally, the system's length should be minimized to maximize the counterweight's movement range.

To meet these design criteria, the actuator in Figure 7 was developed. It uses a servo to turn a spool, which moves a string through pulleys to convert rotational motion into linear movement. The spool has two compartments, each with a string attached. The string in the top compartment passes through a pulley to align with the actuator's cylinder axis, attaching to the bottom of the counterweight. The string in the bottom compartment is recentered by another pulley, running through a carbon tube and a pulley at the end of the actuator, before attaching to the top of the counterweight. When the servo rotates clockwise, the top string winds onto the spool and the bottom string unwinds, moving the counterweight downward (negative $p_{i\text{CM}}$). Counterclockwise rotation moves the counterweight upward (positive $p_{i\text{CM}}$).

E. Aerial platform design

In addition to the novel manipulator design a custom aerial platform was developed specifically for this manipulator morphology. A tradeoff table was used to select the configuration of the drone by selecting relevant criteria, adding a weight (between 1 and 5) and scoring each concept on the criteria (ranging between 1 and 3). The possible drone configurations selected for the tradeoff are tricopter, Y-4 quadrotor, quadcopter, and hexacopter. Under-actuated configurations were selected as these would benefit the most from a force-balanced manipulator. Ease of integration is the first criterion and is scored with a weight of 5. This criterion represents how compatible the drone configuration is with the manipulator morphology. The second criterion is the complexity of the drone configuration which is weighed 3. Since the manipulator

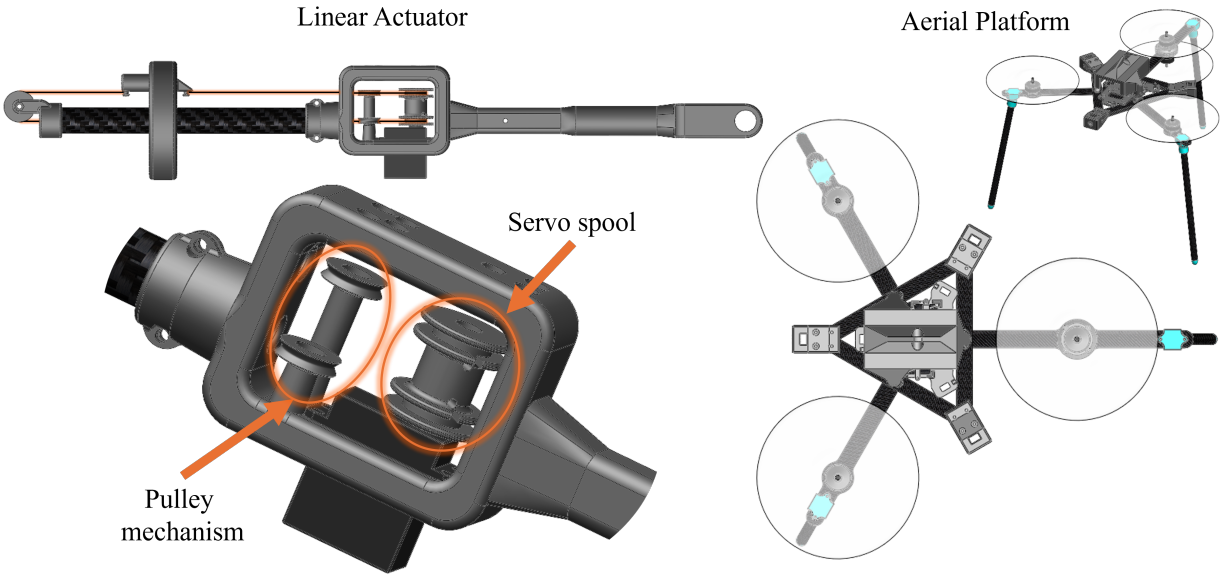

Fig. 7: Render details of the fast linear actuator (left) and the aerial platform (right).

requires nine servos to work the complexity required to manufacture and set up the aerial needs to be minimized. Finally, the last criterion is the cost for each platform, based on the quantity of required components. This criterion is weighed 3. The resulting trade-off table is shown in Table I.

The Y4 quadrotor configuration won the tradeoff as its three-arm morphology leaves most clearance to the three manipulator legs, the complexity is low as similarly to the quadcopter it only requires four motors and electronic speed controllers (ESCs) which limits cable routing issues. For the same reason, the cost of the required components is satisfactory. The tricopter configuration scores similarly in the ease of integration and cost criteria but since the yaw is controlled by angling the back rotor using a servo the complexity is scored low. Finally, the hexacopter configuration requires more components and does not benefit the ease of integration due to the six required arms and therefore scores the lowest.

With the aerial platform selected and the manipulator design completed an initial estimate for the maximum weight of the entire aerial manipulator was calculated. From this estimate, the drivetrain of the aerial platform was sized using a minimum required thrust-to-weight ratio of 2.

TABLE I: Tradeoff table for the selection of the aerial platform configuration.

	Weight	**Tricopter**	**Y4**	**Quadcopter**	**Hexacopter**
Ease of Integration	5	3	3	1	2
Complexity	3	1	3	3	2
Cost	3	3	2	2	1
Score	NA	27	30	20	19

The frame of the aerial platform consists of a triangular-like equilateral frame where the vertexes are the attachment points for the pantographs. The arms for the motors span from the center of the frame through the midpoints of the sides of the triangular frame. The front two arms span 260 [mm] whereas the back arm which has the coaxial motor configuration spans an extra 75 [mm] to account for the landing gear clearance. The motors are mounted at a distance of 200 [mm] from the center of the base. The top and trimeric views of the custom aerial platform are shown in Figure 7.

F. Control

A custom ROS2 (Humble) code base, running on an Orange Pi, was developed to control both the drone platform and manipulator. The Pixracer flight controller on the aerial platform runs the PX4 flight stack and receives position estimates from the Mocap Optitrack system via the Orange Pi. The manipulator and linear actuators are controlled through a ROS2 node, which sends arming, position, and speed commands to a servo driver node. This node communicates with the Teensy microcontroller via UART, which uses asynchronous serial communication to send commands and receive feedback from the servos. The servo feedback is then sent back to the manipulator controller to complete the loop.

A Finite State Machine (FSM), shown in Figure 8, was developed to initialize and control the manipulator and linear actuators. The manipulator controller has two phases: initialization and execution.

Initialization Phase:

- **Arm:** The controller requests an arming command from the user. If received, the servos lock the end-effector in place.

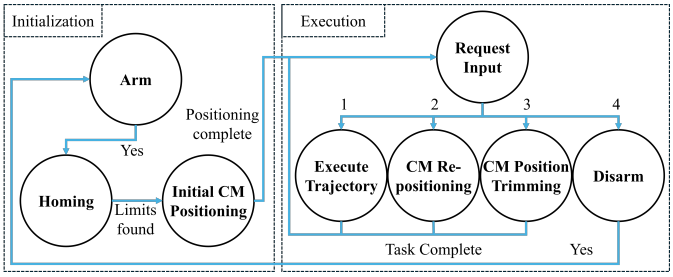

Fig. 8: Finite State Machine diagram for the control of the robotic manipulator. The FSM has two phases: an initialization phase, which manages arming, linear actuator homing, and initial counter-mass positioning; and an execution phase, where the user can request actions such as trajectory execution, counter-mass repositioning, position trimming, and disarming.

- **Homing:** All six linear actuators simultaneously perform a homing procedure to identify counter mass position limits. This is done by moving the counter mass in both directions and using the load feedback to identify the limit. This procedure is necessary as the servos encoders only provide feedback between 0 and 360 degrees.
- **Initial CM Positioning:** Using the equations from subsection III-C, the required counter mass positions are calculated and converted from the reference frame to servo positions interpolating between the known geometric limits of the actuator and the measured position limits of the servo. The servos are controlled through speed commands via a proportional controller.

Execution Phase:

- **Request Input:** The user inputs the desired next state.
- **Execute Trajectory:** The end-effector follows a precomputed trajectory. The inverse kinematics of each setpoint are solved numerically (as described in subsection III-A) and saved onto a file read by the manipulator controller which sends the desired servo angles to the servos. The next trajectory setpoint is published when the error between the actual and desired servo angles falls below a threshold.
- **CM Repositioning:** The counter masses are repositioned based on a new payload inputted by the user.
- **CM Position Trimming:** The counter mass positions are adjusted individually by a desired distance inputted by the user.
- **Disarm:** The servos are disarmed and the system returns to the arm state. After initialization, subsequent arming commands skip the homing and initial CM positioning states, as they are already saved.

IV. Experiments

Two sets of experiment setups were performed to test the performance of the aerial manipulator. The first consists of hanging the system using three ropes to mimic a floating base. This setup is used to evaluate the force-balancing performance

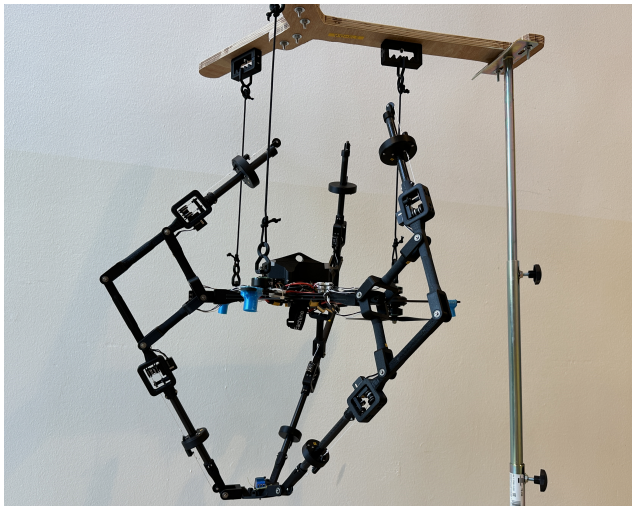

Fig. 9: Floating base experiment setup showcasing the aerial manipulator hanging from three ropes, allowing the whole system to sway horizontally.

of the manipulator. The second series of tests has the aerial manipulator flying in a hover. These tests were performed to evaluate the influence of disturbances generated by the end-effector movement on the position tracking of the aerial platform. The results from these two setups are presented in the following two subsections.

A. Floating experiments

The aerial manipulator is suspended from a custom platform by cables, allowing the system to swing laterally. The accelerations introduced by the end-effector movement on the floating base are recorded from the Pixracer flight controller's accelerometer. Using this setup, the manipulator performs a predefined end-effector trajectory, and the accelerations are logged for analysis. The force-balancing performance of the manipulator is then evaluated by comparing four configurations: unbalanced, balanced, unbalanced with payload, and balanced with payload.

- **Unbalanced:** The manipulator with all counterweights removed.
- **Balanced:** The force-balanced configuration with no payload.
- **Unbalanced with Payload:** The same as the unbalanced configuration, but with a 53 g payload attached to the end-effector. This configuration is not force-balanced, as the counterweights are not adjusted to their balanced position.
- **Balanced with Payload:** The force-balanced configuration, adjusted for the 53 g payload.

For all four configurations three different end-effector trajectories were performed, a line trajectory in the x-direction (in the manipulator coordinate frame of reference), a line in the y-direction and a square trajectory on the X/Y plane. The line trajectories were performed at a z coordinate of 275 [mm] and extended from -100 [mm] to 100 [mm]. The square

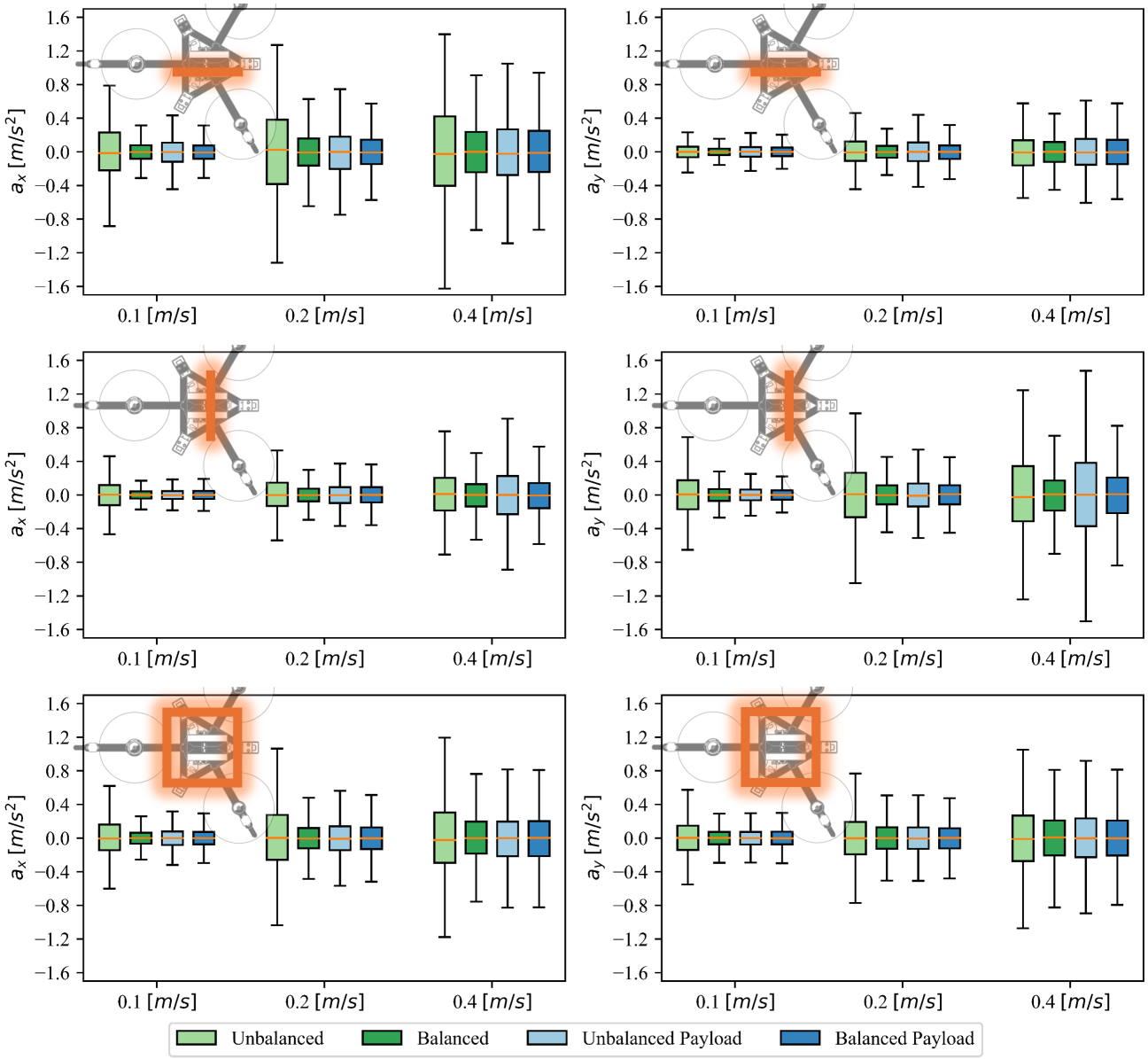

Fig. 10: Box plots for floating base tests showcasing the measured acceleration in x (first column of subplots) and y (second column of subplots) directions for a line trajectory in the x direction (first row), a line trajectory in the y direction (second row) and a square trajectory in the x-y plane (third row). Each trajectory was performed for each configuration of the manipulator (unbalanced, balanced, unbalanced with payload and balanced with payload) and three different end-effector speeds (0.1, 0.2 and 0.4 $[m/s]$). From this figure, we can see that the measured accelerations generally increase for end-effector speed and that the balanced configurations produce lower accelerations than the unbalanced ones.

trajectory was performed at a z coordinate of 300 [mm] with the following vertex (x,y) locations, (-100,-100), (100,-100), (100,100), (-100,100) [mm]. Each trajectory was performed for three different average end-effector speeds, 0.1 $[m/s]$, 0.2 $[m/s]$, and 0.4 $[m/s]$. A boxplot comparing the accelerations for different manipulator configurations in the x and y directions is shown in Figure 10.

In Figure 10 the first row of boxplots shows the results for the tests performing the line trajectory in x direction, the second row of plots shows the results for the line in y trajectory, and the last row presents the results for the square trajectory on the X/Y plane. The first and second columns of subplots show the measured and mean corrected accelerations in the x direction and y direction respectively.

From these results, it is evident that the measured accelerations increase when the end-effector speed increases. As end-effector speed increases, the acceleration to reach successive end-effector position setpoints also increases, producing larger

reaction forces on the manipulator base. This is reflected in the measured accelerations. By looking at each individual manipulator configuration at increasing speeds, we see that the interquartile range and the range of whiskers increase. This behaviour is reflected in all trajectories and for both the acceleration components in x and y.

Furthermore, this figure shows that the measured accelerations decrease between the unbalanced configuration and its balanced counterpart. This is also seen for configurations with payload. Although the accelerations produced by the balanced configurations are not zero a significant decrease is shown therefore demonstrating that the manipulator has force-balancing capabilities. It can also be seen that when adding a payload to the balanced manipulator configured for a payload of 0 [g] the measured acceleration also increases as the manipulator is no longer balanced.

Looking at the magnitude of the accelerations we can also see that for the trajectory in the x direction, the magnitude of measured accelerations is largest in the x direction. This is also seen for the line trajectory in the y direction. For the square trajectory as expected the magnitude of accelerations in the x and y directions are similar.

In addition to the manipulator being force-balanced, it must also be statically balanced. This means that a statically balanced object remains stationary without the need for any braking force such as friction. When the manipulator is in a non-balanced configuration the end-effector drops, fully extending the pantographs. To verify whether the manipulator is statically balanced the counter masses are moved to their balancing locations and the end-effector is moved around its workspace. From this simple test, it was shown that the end-effector remains in the last location it is placed meaning that the manipulator is indeed statically balanced. This test was also repeated adding a payload mass to the end-effector and by reconfiguring the counter mass positions the manipulator also remains statically balanced.

B. Flight experiments

Similar end-effector trajectory tracking experiments were performed with the aerial manipulator in flight. The drone is fixed to hover in position at a height of 1 meter from the ground. Position estimates from the Opitrack system for both the drone position and the end-effector position were collected. The same four manipulator configurations were tested. However, to account for the additional weight of the structure supporting the reflective markers for end-effector position tracking, only a 35 [g] payload was used.

Two trajectories were performed, a square trajectory on the X/Y plane and a line trajectory in the z direction. The square trajectory was performed at a z coordinate of 350 [mm] with (x,y) vertex coordinates: (-80,-80), (80,-80), (80,80), (-80,80) [mm]. The line trajectory in the z-direction ranged between 300 and 400 [mm].

The results for the square trajectory and the line trajectory in z are shown in Figure 11 and Figure 12 respectively.

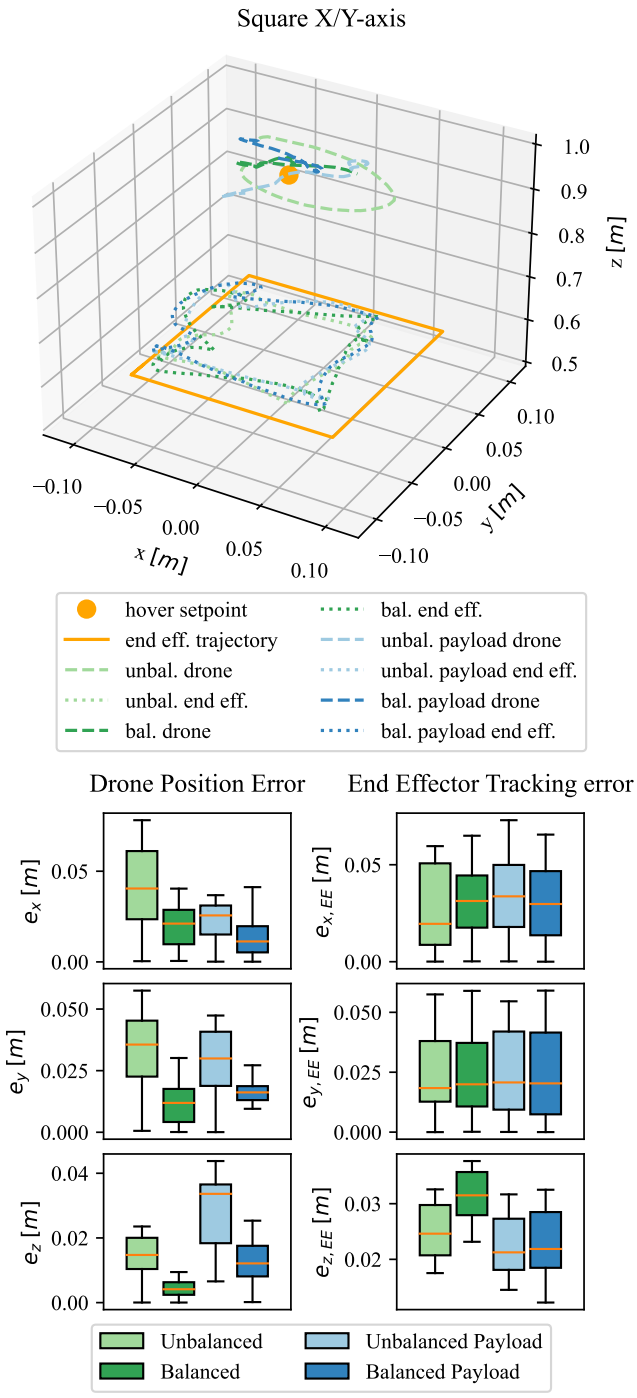

Fig. 11: Position plot and Box plots for a flying test performing a square trajectory on the x-y plane. These plots showcase the results for all four manipulator configurations (unbalanced, balanced, unbalanced with payload and balanced with payload) at a 0.1 $[m/s]$ end-effector speed. For clarity, only one repetition of the trajectory is showcased in the 3d plot. The figure shows improved drone position tracking for balanced manipulator configurations compared to their unbalanced counterparts.

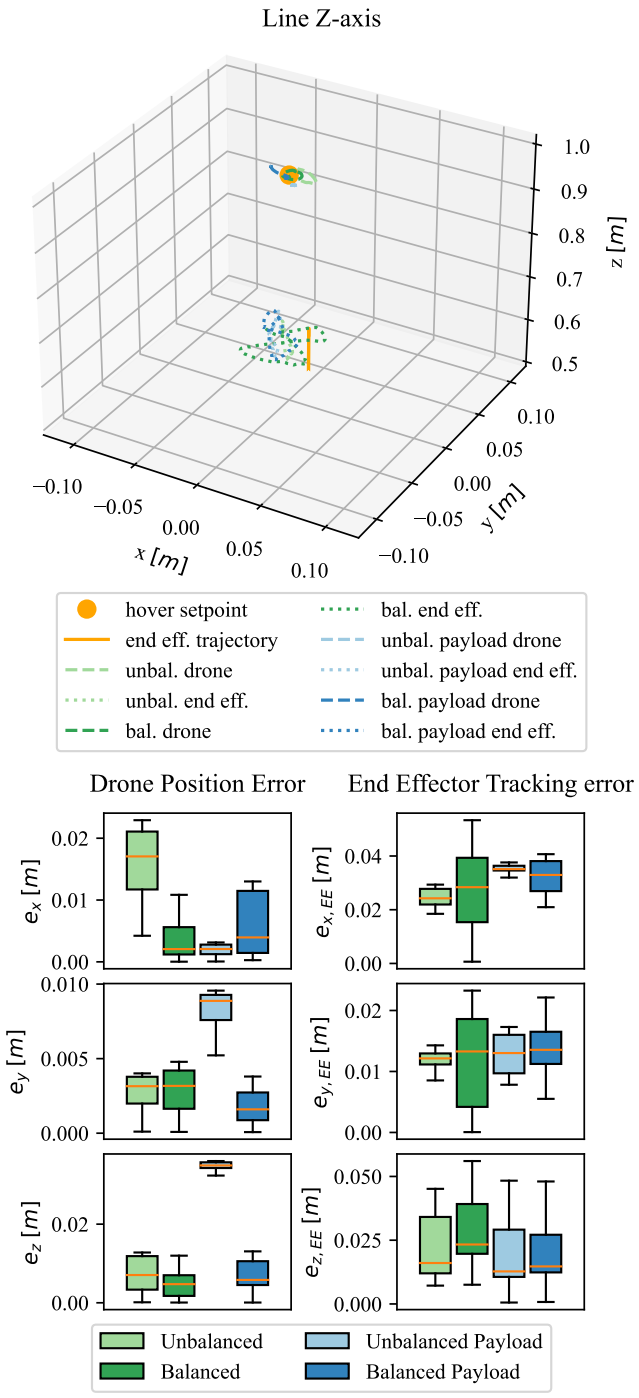

Fig. 12: Position plot and Box plots for a flying test performing a line trajectory in the z-direction. These plots showcase the results for all four manipulator configurations (unbalanced, balanced, unbalanced with payload and balanced with payload) at a 0.1 $[m/s]$ end-effector speed. For clarity, only one repetition of the trajectory is showcased in the 3d plot. The figure shows improved drone position tracking for balanced manipulator configurations compared to their unbalanced counterparts.

Both figures present a scatter plot at the top of the figure with the desired position and true position tracking of both the drone and end-effector. For clarity, only one repetition of the trajectory is showcased. The bottom part of the figures contains boxplots displaying the absolute position error (absolute value of the desired position minus true position) in x, y, and z.

From the square trajectory results presented in Figure 11 we can see that the absolute position tracking error for the drone platform in all directions is larger for the unbalanced configurations compared to their balanced counterpart. Furthermore, the tracking error in z is particularly larger for the unbalanced configuration with the payload. This shows that the force-balanced configurations reduce the disturbances introduced to the aerial platform, yielding better position-tracking results.

The end-effector tracking error is calculated by subtracting the drone position error from the true end-effector position. This is because the end-effector position setpoint is considered fixed with respect to the drone's hover position setpoint, meaning that the drone position errors also affect the end-effector position measurement. As expected this error is consistent across manipulator configurations. This is because the end-effector error is a systematic error resulting from kinematic inaccuracies from imperfect manufacturing.

From the line trajectory in the z direction results presented in Figure 12 similar conclusions to the square trajectory can be made. For the z direction, the drone position error decreases when comparing the unbalanced configuration to its balanced configuration. For the two other directions, this is not always the case however excluding the error in the x direction for the unbalanced configuration the position error magnitudes are lower than the error in the z direction. This is likely because we are measuring mostly the drone controller's inherent tracking error.

For the z direction, the difference is mostly noticeable between the unbalanced and balanced configurations with payload. This highlights the necessity of being able to reconfigure the manipulator for different payloads.

Similarly to the square trajectory results the end-effector tracking error is also consistent across manipulator configurations.

Finally, the mean and standard deviation for the drone's and the end-effector's absolute position errors are presented in the table below. These statistics are computed for a complete trajectory with movement in all axes. The trajectory first performs a line in the z direction, then a line in the x direction followed by a line in the y direction. lastly, a square trajectory on the X/Y plane is performed. Each trajectory is repeated three times.

From these results, it is easier to see that the force-balanced configurations are successful in reducing the drone position tracking error. Between the unbalanced and balanced configurations, a 19% decrease in the error was noticed and between the unbalanced and balanced configurations carrying the payload a 34% decrease in the error was noticed. Regarding, the end-effector tracking the errors are consistent across different manipulator configurations again highlighting

TABLE II: Mean and standard deviation of the drone and the end-effector position tracking errors. The results provided in this table show improved drone position tracking for balanced manipulator configurations compared to their unbalanced counterparts.

		Unbalanced	Balanced	Unbalanced payload	Balanced payload
Drone position error	mean [m]	0.043	0.035	0.047	0.031
	std [m]	0.021	0.014	0.015	0.016
End-effector position error	mean [m]	0.047	0.051	0.048	0.049
	std [m]	0.016	0.013	0.015	0.016

that the imperfect mechanical construction of the manipulator produces a systematic error.

V. Design lessons

The results presented in section IV demonstrate that the manipulator developed is force-balanced and is capable of reconfiguring itself to maintain its force-balancing properties for different payloads. Furthermore, in the force-balanced configurations, the aerial manipulator yields better position-tracking. This design, however, is not perfect as in the floating base tests it did not reduce the measured accelerations to zero and during the flight experiments it was noticed that the end-effector tracking contained noticeable errors.

During testing, it was noticed that the quality of construction and specifically the alignment of the pantographs greatly affects the force-balancing performance of the manipulator and the end-effector tracking. The material used, PAHT-CF, has a high moisture absorption rate. During printing of the main joint components for the pantograph mechanism, these would tend to warp due to their elongated shape. Although immediately after printing these parts were clamped between two straight surfaces to straighten them, with time as the parts absorbed moisture the warping would return. A future redesign could benefit from using another filament such as carbon-reinforced PLA or even manufacturing the parts out of aluminum, although the latter will require a significant redesign of the joints.

The end-effector occasionally loses parallel alignment with its base, affecting its overall tracking performance. This was noticed mostly for higher-speed trajectories likely because the end-effector position setpoints are spaced further apart to achieve the higher end-effector speed. Whilst moving between setpoints the manipulator may enter a mixed freedom mode of operation which allows for the tilt of the end-effector platform. This should occur when the z axis of the end-effector platform and the z axis of the base coincide however it was also noticed when the end-effector was not in this condition. Furthermore, this switching between operating modes was more prevalent during tests where the counter masses were removed. This may be due to the mass distribution of the unbalanced pantograph mechanism. This issue could be improved by solving the Jacobian of the kinematics and developing a controller which controls the joint speed instead of the joint position. In addition, better manufacturing of the pantographs could also limit this undesired switching between operating modes.

The balancing performance is also very sensitive to the counter mass positions hence these were often manually tweaked until static balancing of the manipulator was reached. This was exacerbated by the homing position limits often varying between homing sequences. This is because there is backlash in the linear actuators when the counter mass is starting to touch a limit. Stretch in the string makes it such the servo rotates further than required producing this inconsistency between different homing procedures. In addition, this makes it such that the desired counter mass position is not exactly the one reached in reality. Further work on the linear actuator and homing sequence would yield better results. This can be done by using a different string such as a kevlar which has less stretch or fine-tuning even further the limit detection.

Furthermore, one of the assumptions in subsection III-C is that the COM for the pantograph links lies in the same axis as the link ($q_1, q_2, q_3, q_4 = 0$). This assumption, however, is not true as the servo and servo joint for the linear actuator is offset with respect to the links axis. The COM is nevertheless close to this axis but an improvement could be to place a counter mass opposite to the servo to ensure the assumption holds. This could lead to potentially better results.

Finally, once a payload is picked up the position of the payload cog is not equivalent to the one of end effector which also breaks the assumption that the weight at the end-effector is located at the end-effector kinematic origin. This can be easily integrated as an input to the force-balancing equations governing the position of the counter masses.

VI. Conclusions

This work presents the design, fabrication and testing of a novel aerial manipulator equipped with a reconfigurable force-balanced manipulator. The design of the force-balanced manipulator, a custom linear actuator, a custom aerial platform, a control architecture for the entire system, and the fabrication of the system were described. Testing on a floating base setup demonstrated the manipulator being statically and force-balanced. Tests with the system hovering demonstrated significant improvement in the position tracking of the drone whilst being disturbed due to end-effector movements. Design lessons and future recommendations were discussed for better end-effector position tracking and to further enhance the force-balancing quality of the manipulator. In conclusion, this paper showcased that a smart mechanical design for the manipulator is capable of improving the performance of an aerial manipulator without requiring complex control of the aerial platform.

References

[1] Salua Hamaza et al. "Sensor Installation and Retrieval Operations Using an Unmanned Aerial Manipulator". In: *IEEE Robotics and Automation Letters* 4.3 (2019), pp. 2793–2800.

[2] Miguel Ángel Trujillo et al. "Novel Aerial Manipulator for Accurate and Robust Industrial NDT Contact Inspection: A New Tool for the Oil and Gas Inspection Industry". In: *Sensors* 19.6 (2019).

[3] Pisak Chermprayong et al. "An Integrated Delta Manipulator for Aerial Repair: A New Aerial Robotic System". In: *IEEE Robotics Automation Magazine* 26.1 (2019), pp. 54–66.

[4] Micha Schuster et al. "Automated Aerial Screwing with a Fully Actuated Aerial Manipulator". In: *2022 IEEE/RSJ International Conference on Intelligent Robots and Systems (IROS)*. 2022, pp. 3340–3347.

[5] Alejandro Suárez et al. "Through-Window Home Aerial Delivery System with In-Flight Parcel Load and Handover: Design and Validation in Indoor Scenario". In: *International Journal of Social Robotics* (Oct. 2024), pp. 1–24.

[6] Fabio Ruggiero, Vincenzo Lippiello, and Anibal Ollero. "Aerial Manipulation: A Literature Review". In: *IEEE Robotics and Automation Letters* 3.3 (2018), pp. 1957–1964.

[7] Caiwu Ding and Lu Lu. "A Tilting-Rotor Unmanned Aerial Vehicle for Enhanced Aerial Locomotion and Manipulation Capabilities: Design, Control, and Applications". In: *IEEE/ASME Transactions on Mechatronics* 26.4 (2021), pp. 2237–2248.

[8] Carmine Dario Bellicoso et al. "Design, modeling and control of a 5-DoF light-weight robot arm for aerial manipulation". In: *2015 23rd Mediterranean Conference on Control and Automation (MED)*. 2015, pp. 853–858.

[9] Salua Hamaza and Mirko Kovac. "Omni-Drone: on the Design of a Novel Aerial Manipulator with Omnidirectional Workspace". In: *2020 17th International Conference on Ubiquitous Robots (UR)*. 2020, pp. 153–158.

[10] Nursultan Imanberdiyev et al. "Design, development and experimental validation of a lightweight dual-arm aerial manipulator with a COG balancing mechanism". In: *Mechatronics* 82 (2022), p. 102719.

[11] Ayham AlAkhras et al. "The Design of a Lightweight Cable Aerial Manipulator with a CoG Compensation Mechanism for Construction Inspection Purposes". In: *Applied Sciences* 12.3 (2022).

[12] Ibrahim Abuzayed et al. "Design of Lightweight Aerial Manipulator with a CoG Compensation Mechanism". In: *2020 Advances in Science and Engineering Technology International Conferences (ASET)*. 2020, pp. 1–5.

[13] Volkert van der Wijk and Just Herder. "Dynamic Balancing of Clavel's Delta Robot". In: Jan. 2009, pp. 315–322. ISBN: 978-3-642-01946-3.

[14] Yangnian Wu and C. Gosselin. "Design of reactionless 3-DOF and 6-DOF parallel manipulators using parallelepiped mechanisms". In: *IEEE Transactions on Robotics* 21.5 (2005), pp. 821–833.

[15] Sébastien Briot, Vigen Arakelian, and Sylvain Guégan. "PAMINSA: A new family of partially decoupled parallel manipulators". In: *Mechanism and Machine Theory* 44.2 (2009), pp. 425–444. ISSN: 0094-114X.

[16] Kartik Suryavanshi et al. "ADAPT: A 3 Degrees of Freedom Reconfigurable Force Balanced Parallel Manipulator for Aerial Applications". In: *2023 IEEE International Conference on Robotics and Automation (ICRA)*. 2023, pp. 11936–11942.

[17] Angus B. Clark et al. "On a Balanced Delta Robot for Precise Aerial Manipulation: Implementation, Testing, and Lessons for Future Designs". In: *2022 IEEE/RSJ International Conference on Intelligent Robots and Systems (IROS)*. 2022, pp. 7359–7366.

[18] Jan Jong and Just Herder. "A comparison between five principle strategies for adapting shaking force balance during varying payload". In: Oct. 2015.

[19] Eduardo Castillo Castaneda et al. "Delta robot: Inverse, direct, and intermediate Jacobians". In: *Proceedings of The Institution of Mechanical Engineers Part C-journal of Mechanical Engineering Science - PROC INST MECH ENG C-J MECH E* 220 (Mar. 2006), pp. 103–109.

[20] Yangmin Li. "Kinematic Analysis and Design of a New 3DOF Translational Parallel Manipulator". In: *Journal of Mechanical Design - J MECH DESIGN* 128 (July 2006).

[21] Volkert van der Wijk. "Methodology for analysis and synthesis of inherently force and moment-balanced mechanisms". In: 2014. URL: https://api.semanticscholar.org/CorpusID:108060903.

APPENDIX

The following appendix describes the fabrication of the different components making up the reconfigurable force-balanced aerial manipulator.

A. Aerial Platform

The aerial platform is fabricated by waterjet cut carbon fiber plates, 4 [mm] thick for the motor arms and 2 sandwiched 2 [mm] thick plates for the manipulator frame. The coaxial motor mount, electronics mounts and cover are 3-D printed out of PAHT-CF material on the Bambu Lab Carbon X1 printer. The linear actuator shaft is made of 14 [mm] outer and 10 [mm] inner diameter carbon fiber tube. The landing gear is also manufactured from the same dimension carbon fiber tube. The landing gear joints and feet are made out of TPU 95A to be more compliant and absorb the impact of harder landings.

B. Robotic Manipulator

Each joint and component of the manipulator is 3-D printed out of PAHT-CF material. This excludes the linear actuator shaft which is made of 14 [mm] outer and 10 [mm] inner diameter carbon fiber tube and the counter masses which are made out of PLA. Bearings were used for every passive joint and the linear actuator pulleys to reduce friction in the manipulator movement.

Each pantograph is composed of 15 3D printed parts, three servos, some string for the linear actuator and 2M hardware. During assembly, the mass of each component was measured and the final parameters defining the force-balancing properties of the manipulator are reported in Table III.

TABLE III: Measured parameters of the force-balanced manipulator.

	Pantograph 1	**Pantograph 2**	**Pantograph 3**
$\widehat{m}_1$ [g]	135.2	135.0	134.7
$\hat{p}_1$ [mm]	132.2	132.3	132.5
$m_{1\mathrm{CM}}$ [g]	56.0	56.0	56.0
$\widehat{m}_2$ [g]	99.1	98.6	98.8
$\hat{p}_2$ [mm]	51.7	51.7	51.5
$m_{2\mathrm{CM}}$ [g]	114.0	114.1	114.0
m_3 [g]	32.3	32.4	32.5
p_3 [mm]	68.1	68.4	68.4
m_4 [g]	31.3	31.2	31.2
p_4 [mm]	69.1	69.0	69.1
m_{total} [g]	467.9	467.3	467.2
$m_{man.}$ [g]		1402.4	

To add the required mass to the counter masses 2.71 mm diameter bearing balls were used. The counter mass consists of three components: a container, a lid and a tightening mechanism. The bearing balls are contained within the container and lid. The tightening mechanism is used to increase tension on the string which drives the counter mass motion.

C. Electronics

The electronics used to control the aerial manipulator are an Orange pi 5 for the onboard computing, the mRo Pixracer r15 as the flight controller, the Teensy 4.0 micro-controller which handles the communication with the servos, and the FrSky R-XSR receiver to control the vehicle through remote control (RC). The servos used are the Feetech STS3032 servos and they are used both for the linear actuator and the manipulator movement. As the manipulator is designed to perform pick-and-place tasks, the end-effector is outfitted with a small electromagnet and relay switch. To power the Orange Pi 5 and the Pixracer the CastleCreations 10 amp BEC is used. The servos and electromagnet instead are powered through a 12 amp UBEC. These components and the ESCs receive power directly from the battery through a custom wire harness. For battery monitoring, a voltage checker is directly connected to the balance port of the battery.

The drivetrain of the drone is as follows: The motor and propeller combination selected are the T-motor Velox 2808 1500kv motors and Gemfan 8040-3 propellers which produce 985.8 [g] of thrust at 40% throttle and 25.1 [V]. The motors are capable of drawing 70 amps of current at max throttle therefore the 70 amp DYS AM32 Aria ESCs were selected. To power the entire system a 6s 6000 mah battery was selected which yields an estimated flight time of 10 minutes.

[This page is intentionally left blank]

Part III

Literature Review

*This part has been assessed for the course AE4020 Literature Study.

[This page is intentionally left blank]

Active Force Balanced Delta Manipulator for Dynamic Pick-and-Place Tasks

AE4020: Literature Study

Michele Bianconi

Delft University of Technology

TU Delft

Active Force Balanced Delta Manipulator for Dynamic Pick-and-Place Tasks

by

Student Name	Student Number
Bianconi Michele	4857771

Main Instructor:	S. Hamaza
Institution:	Delft University of Technology
Place:	Faculty of Aerospace Engineering, Delft
Project Duration:	March - August, 2023

TU Delft

Contents

Nomenclature

Abbreviations

Abbreviation	Definition
ADBB	Active Dynamic Balancing Blocks
CAGR	Compound Annual Growth Rate
CoG	Centre of Gravity
CRCM	Counter Rotary Counter Masses
DoF(s)	Degree(s) of Freedom
FDM	Fused Deposition Modelling
GNSS	Global Navigation Sensing System
(I)NDI	(Incremental) Nonlinear Dynamic Inversion
PID	Proportional Integral Derivative
SLAM	Simultaneous Localisation and Mapping
UAM	Unmanned Aerial Manipulator
UAV	Unmanned Aerial Vehicle
VTOL	Vertical Takeoff and Landing

List of Figures

1 Introduction

The miniaturization of electronics[7] and the improvement of electrical power supplies, such as the development of lithium-based batteries[62], promoted vast advancements in Unmanned Aerial Vehicles (UAVs). UAVs, commonly referred to as drones, are defined as ”aircraft that can navigate without a human pilot on board”[22]. This class of aircraft has multiple uses both in the military and civil sectors such as law enforcement[12], surveillance[33], filmmaking [54], environmental monitoring[44], cargo transport[28], search and rescue[24], and agriculture[23]. The global market for UAVs has shown remarkable growth and is expected to keep growing with an expected Compound Annual Growth Rate (CAGR) of around 10% in this decade[59][29].

With the development of new UAV systems and with their increase in applications the field of Unmanned Aerial Manipulation, also referred to as Aerial Manipulation, has seen sustained growth during the past decade[63]. Aerial manipulation encompasses ”aerial robots equipped with robotic manipulators to perform tasks”[67]. Typically UAV systems have been employed in sensing tasks but more research is currently being done to use UAVs for contact-based tasks.

Examples of applications for aerial manipulators are non-destructive testing [1], aerial repair [16], load transportation [8], inspection [75], sensor installation [34] and more. These systems now allow UAVs to perform more interactive roles and are bringing forth new and more complex morphologies of aerial vehicles.

The purpose of this report is to identify a knowledge gap in the field of aerial manipulation and what novel designs are yet to be explored. The goal is to search for design opportunities which consider a smart design approach which views aerial manipulators as an individual system instead of a simple combination of a UAV with a robotic arm. Current research will be analysed to determine what morphologies and design approaches can yield a novel and well-integrated aerial manipulator.

1.1. Research Question

To further expand the research in the field of aerial manipulation the following research question was formulated. This research question is further divided into subquestions to more easily identify concrete solutions which can answer the main question.

How can a smart mechanical design limit coupling effects between the individual subsystems of an aerial manipulator and be paired with a control scheme to perform dynamic pick-and-place tasks requiring fast manipulator movements?

- What manipulation task would be well-suited to showcase the benefits of an innovative aerial manipulation system?
- What type of manipulator morphologies would limit the effect of dynamic end effector movements on its base and how can this be integrated with an aerial platform to achieve a streamlined design?
- How can state-of-the-art force balancing mechanisms be adapted to tasks with time-varying payloads?
- What type of aerial platform would benefit the most from an active force balancing system, eg. quadrotor, tiltrotor etc.?
- What control approach is best suited for a well-integrated force-balanced aerial manipulator?

1.2. Content Outline

This literature review is divided into four chapters. Chapter 2 provides a general introduction, a brief history, and current developments in the field of aerial manipulation. Furthermore, it discusses the different tasks tackled by aerial manipulators. Chapter 3 discusses the working principle of robotic manipulators, the two types of robotic manipulators, a special category of manipulator mechanisms and grippers typically used for pick-and-place tasks. Chapter 4 presents the different types of aerial platforms used in aerial manipulation and their actuation capabilities. Chapter 5 presents the two control approaches in aerial manipulation and different position controllers for aerial platforms. Finally, Chapter 6 provides a conclusion to the literature review.

2
Aerial Manipulation

Research in the field of aerial manipulation has seen a constant influx of publications including multiple literature reviews[63][70] and a book[67], consolidating this as an essential and independent field of research. The following sections aim to give a general introduction to the field of aerial manipulation and what work has been published by the community.

This chapter begins with a brief history of aerial manipulation in Section 2.1, followed by the different tasks performed by aerial manipulators in Section 2.2.

2.1. Brief History

Physical interactions between the environment and aerial systems have been accomplished in the past by manned aircraft such as slung load transportation by helicopters and air-to-air refuelling. These applications originally laid the groundwork to perform physical interaction tasks using unmanned aerial systems.

2.1.1. Flying Hands

Flying hands, namely aerial vehicles for which the payload cannot be moved independently from the drone, constituted new developments for aerial manipulation. This class of aerial manipulators can be subdivided into two classes: platforms with tether/cable mechanisms and platforms with grippers attached to the aerial frame.

Slung load transportation is an example of a platform with a cable mechanism. This application has been achieved using unmanned autonomous helicopters as presented in the article by Bernard et al. [8] where the authors described a control approach for load transportation. The algorithm showcased could work for single or multiple coupled helicopters. This work was further developed for the application of search and rescue within the framework of the AWARE project which was funded by the European Commission[9]. The accurate deployment of small payloads such as sensors and the slung load transportation by one and three coupled helicopters was showcased in this work.

The European-funded PLANET FP7 project showcased an example of a platform with a gripper directly attached to it[46]. Laiacker et al. worked on an unmanned helicopter solution with a gripper capable of deployment and retrieval of a mobile ground robot. This work employed accurate target location using a camera and a gripper design inspired by the probe-and-drogue aerial refuelling system to retrieve/deploy the ground robot.

Amongst the first uses of multi-rotors as aerial platforms is the work of Albers et al. [4] where a quadrotor was used to apply force to a wall while maintaining flight stability. This type of aerial manipulator may also be classified as a flying hand as it is equipped with a rigid tool whose movement is dependent on the aerial platform.

Furthermore, a quadrotor aerial platform with an attached gripper was used in the work of Mellinger et al. [56]. Their work addressed the design and control for aerial grasping showcasing a design capable of perching on beams or branches and grasping and transporting payloads.

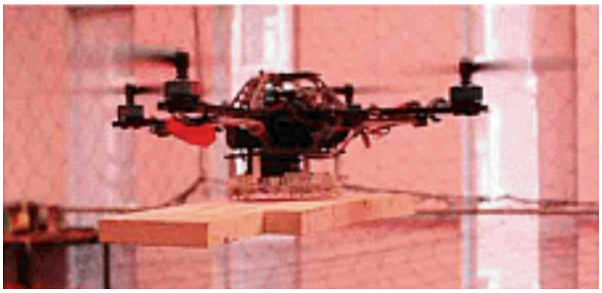

Figure 2.1: Example of a flying hand aerial manipulator from Mellinger et al. [56]

The use of flying hands is not only limited to the grasping and transport of payloads but as Lindsey et al. [51] showed such aerial vehicles can also be employed in the construction of simple structures. In their work, they used a quadrotor equipped with a gripper to pick up, transport and assemble a structure out of basic members and node blocks. They developed a control algorithm capable of coordinating multiple quadrotors to perform the assembly of structures.

2.1.2. First Generation Aerial Manipulators

With flying hands, the only possible tasks are pick-and-place or load application to the environment and the accuracy of such tasks is fully dependent on the accuracy of the position control and stability performance of the aerial platform. Hence, to overcome these limitations aerial platforms have been combined with multiple Degrees Of Freedom (DoFs) robotic manipulators. This type of aerial manipulator is more complex but the manipulation capability is no longer solely dependent on the aerial platform.

Amongst the first aerial manipulators equipped with multiple DoFs robotic manipulators is the work of Suseong et al.[41]. They presented a quadrotor with a two-DoF robot arm capable of picking and placing a wooden block within a shelf. Such a task would not be possible with flying hand vehicles such as the ones previously presented.

Another example is the work of Fumagalli et al. who designed a different aerial manipulator equipping a three-DoF delta manipulator on a quadrotor platform[30]. This aerial manipulator was designed to carry out physical interaction tasks for aerial inspection of industrial plants. Their work showcased that the end effector position error is decreased with the active manipulator compared to its fixed configuration relying only on the aerial platform's position controller. Furthermore, their design was capable of applying forces on the environment while maintaining flight stability.

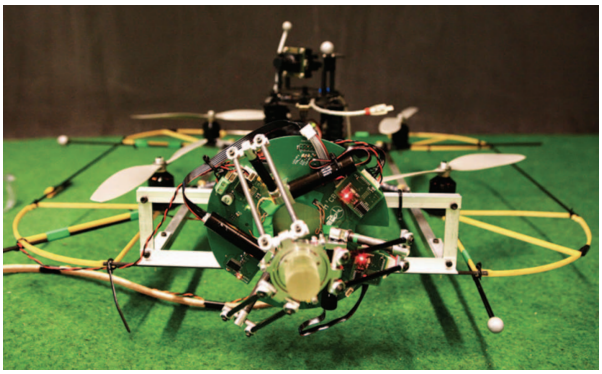

Figure 2.2: Example of a first generation aerial manipulator from Fumagalli et al. [30]

Furthermore, helicopters were also equipped with multiple DoF manipulators such as the work by Kondak et al. [43] who combined a helicopter with an industrial seven-DoF serial manipulator. This integration was motivated by the industry's desire for high payload weight and advanced manipulation capabilities, which this type of robotic arm is capable of achieving.

2.1.3. Second Generation Aerial Manipulators

These first types of aerial manipulators equipped with multiple DoF manipulators were mostly developed and tested to work indoors however, soon after efforts were made to adapt these aerial manipulators for outdoor operation such as in [39]. Jimenez-Cano et al. worked on a quadrotor with a multi-link arm for assembly tasks. This aerial manipulator was equipped with a Global Navigation Sensing System (GNSS) and tested outdoors.

Figure 2.3: Example of a second generation aerial manipulator from Jimenez-Cano et al. [39]

Furthermore, Morton et al. [60] developed a framework for an outdoor mobile manipulation UAV. Their work focused on creating an easy-to-modify system which supports multiple aerial vehicles, manipulators and control methods. This was done by designing a hardware and software architecture and multiple other subsystems using a modular framework allowing for robust system expansion.

2.1.4. Current Aerial Manipulators

More recent UAM designs encompass indoor and outdoor operation and more complicated morphologies, multiple arms, and more advanced navigation capabilities. These advances also led to testing more complete and comprehensive real-world applications compared to previous tests mostly showcasing accurate positioning or stability capabilities.

The use of fully-actuated aerial platforms was showcased in the work of Ryll et al. [71] where they developed a six-DoF aerial platform with a rigid end effector. Their work aimed to develop a UAM capable of fully controlling its position and orientation and of exerting forces and torques independently on the environment. This morphology enabled this aerial manipulator to perform tasks which would require a manipulator of multiple DoFs on a traditional multirotor configuration.

In [76] Suarez et al. showcased the design of an aerial manipulator equipped with a dual-arm robotic manipulator. Their work aimed to design a lightweight and compliant manipulator to be used by a multirotor platform. Later, in [79], their design was tested in pipe inspection tasks involving the grasping and installation of sensors and inspection tools.

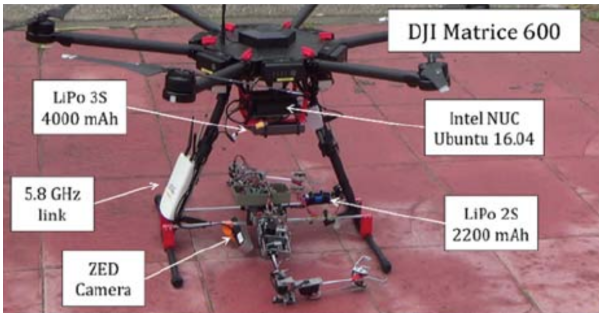

Figure 2.4: Example of a current generation aerial manipulator from Suarez et al. [76]

Another example of developing and using these aerial manipulators for more extensive practical tasks is the work of Chermprayong et al. [16]. They presented an aerial manipulator equipped with a delta manipulator and a foam extruder specifically designed for the aerial repair of pipes by depositing a PU foam.

Since aerial manipulators require accurate localization for manipulation Pumarola et al. developed a new Simultaneous Localisation and Mapping (SLAM) technique called PL-SLAM for the precise localization of aerial manipulators[69]. Their method aimed to improve point-only based methods in scenarios such as poorly textured scenes or motion-blurred images where they perform more poorly.

Furthermore, many works focus on complex control architectures to accurately control aerial manipulators and specifically to model and limit the influence of the manipulator on the aerial platform. Recently a group within the aerial manipulation community has been working on implementing better designs for robotic manipulators to limit this influence. For example, the work of Hamaza et al. presented the design of an aerial manipulator with a parallel robotic arm and an omnidirectional workspace. The mechanical design implemented a moving counterweight mechanism making the system dynamically balanced. This mechanism enables the vehicle to be uninfluenced by the destabilising momentum created by loads on the end-effector.

This design was later showcased in the work of Abu-Jurji et al. who developed a sensorless impedance control scheme for this aerial manipulator for curved surface inspections[1].

2.2. Aerial Manipulation Tasks

Aerial manipulators are designed for multiple applications which require different tasks to be performed. This section classifies typical robotic tasks which are typically tackled in the aerial robotics community. The different tasks described in the following subsections are pick and place, point contact, pulling and pushing, sliding, peg-in-hole, and manipulation. These tasks all focus on the physical interaction between the vehicle's manipulator and the environment.

2.2.1. Pick and Place

The aim of this task is to take, move and put down a movable object. The interaction forces are typically assumed to be negligible as the interaction time of picking and placing is usually short. This specific task has been performed both by flying hands such as the previously mentioned work by Laicker et al. where a helicopter with a gripper would pick up and place a mobile ground robot[46].

More complex manipulators have been used for pick and place tasks such as the work of Garimella et al. where a quadrotor was equipped with a two-DoF manipulator with a gripper[31]. This aerial manipulator was tested in a scenario where it would fly towards a marked point in front of an object and use its manipulator to retrieve it.

2.2.2. Point Contact

Point contact tasks aim to maintain contact between the end-effector of the aerial manipulator and a single point on the environment, for example, a surface. For this type of task, interaction forces are not negligible and many factors affect performance, such as the transition between contact-free and contact

flight, bouncing effects and friction. The aerial manipulator must be capable of correctly applying forces without slippage or destabilizing the aerial platform.

Hamaza et al. presented an aerial manipulator for sensor installation and retrieval[34]. Their work showcased a vehicle capable of placing a sensor on a surface and applying the required force to ensure good adhesion. In addition and for the same reason, the system had to ensure good control of the direction of the force application.

2.2.3. Pulling and Pushing

This task is similar to point contact tasks with the difference that the point of contact is not fixed but moves in space. This presents an additional challenge as the dynamics of the object need to be taken into account. For a pulling task typically the end effector and object are constrained however, for a pushing task this is not necessarily the case and the interaction force generated should be sufficient to generate enough friction.

An example of such a task was presented in [48] where Lee et al. developed an aerial manipulator capable of opening a hinged door. A controller was developed taking into account the simplified coupled dynamics between the UAM and the door. Furthermore, this work considered crash prevention with the moving door and door frame for a collision-free trajectory.

2.2.4. Sliding

For sliding tasks, the aerial manipulator tries to maintain contact between the end-effector and the environment while the end-effector itself is in movement. This task is performed on static surfaces and the effects of static and dynamic friction between the end-effector and the surface must be taken into account to ensure proper trajectory tracking, contact and no slippage.

This type of task has been tackled by Hamaza et al. in [35] where a force controller on an aerial manipulator was implemented for aerial contour follow. This work strived for the aerial manipulator to apply a continuous shear force ensuring the end-effector maintains contact with the surface.

2.2.5. Peg-in-Hole

Peg-in-hole tasks aim to insert an object or the end-effector inside a hole for which the difference in size between the two is small. This task proves challenging as during the inserting motion some of the DoF of the manipulator becomes constrained and high-frequency vibrations and resonant effects can occur.

The work previously presented by Ryll et al. which showcased a fully actuated aerial manipulator with a rigid end-effector was tested on a tilted peg-in-hole task[71]. The aerial manipulator was tasked with inserting and removing its end-effector from a tilted standing funnel, however, the planned trajectory for this manoeuvre expects an upright funnel. This work showcased the system's ability to adapt to an unexpected scenario while performing a complex task.

2.2.6. Manipulation

This category of tasks encompasses physical interaction tasks which require the application of different forces and torques. These tasks often require different manipulators designed specifically for a particular environment with different degrees of complexity. The end-effector as well is also be tailored to the specific task and may be made of soft material or include a spring mechanism such as in the previously cited work of Fumagalli et al. developing a compliant end-effector for aerial inspection[30].

Other examples may be the dual-arm aerial manipulator turning a valve showcased in [65], a tree inspection aerial robot in [75] and the previously mentioned work by Chermprayong et al. for aerial repair in [16].

2.3. Research Opportunity

This chapter discussed a brief history of the work done in the field of aerial manipulation and the different tasks performed by aerial manipulators. The aim of this chapter was to give some context on this field

of research but also to identify a research opportunity to further develop the applications achievable by aerial manipulators.

Referring to the first sub-question in Section 1.1: What manipulation task would be well-suited to showcase the benefits of an innovative aerial manipulation system? it can be reasoned that an innovative aerial manipulator should be able to tackle innovative tasks which require a larger degree of complexity.

As discussed in this chapter the current trend of research is to develop more complex aerial manipulator morphologies, test more realistic scenarios and perform tasks with a strong interaction with the environment. An example is the work of Lee et al. [48] mentioned in Section 2.2.3. A task such as opening a hinged door presents additional challenges as discussed in the section. Tasks such as pick and place are less commonplace compared to the first generations of aerial manipulators.

However, to the best knowledge of the author, pick and place tasks tackled by previous research were all performed statically, meaning the object to be grasped or the surface upon the object rested is static. In order to add a degree of complexity a novel dynamic pick and place task could be tackled where an object is grasped or placed on a moving surface. Such a task would require fast and accurate end effector movements without affecting the stability of the aerial platform.

3
Robotic Manipulators

Robotic manipulation refers to how robots interact with objects in the environment and has been a well-established field for some time. These types of robots are used for various applications such as on production lines in factories, surgery, bomb disposal, marine exploration, and on space vehicles. By attaching robotic manipulators to UAVs the number of locations accessible for robotic manipulation increases leading to new applications for these systems. The following sections discuss robotic manipulators for aerial manipulation.

This chapter begins with a description of the working principles of robotic manipulators in Section 3.1. This is followed by the classification of different manipulator types in Section 3.2. Section 3.3 showcases a specific kind of robotic manipulator which is promising for aerial manipulation. The chapter ends with Section 3.4 briefly explaining grippers used for pick and place tasks.

3.1. Working Principle

Robotic manipulators are robotic mechanisms formed by multiple rigid bodies connected through joints. The mechanical structure of the robotic manipulator is composed of structural elements such as beams, links, castings, shafts, slides, and bearings. Typically, these elements are assumed to be rigid.

The elements of the structure which allow movement are the joints. Typical types of joints are prismatic joints and revolute joints. The first allows linear movement and the second enables rotary movement. Other existing joints are ball-in-socket also known as spherical joints and the Hooke-type universal joints. For the joints to move actuators are used. These can be electric, hydraulic and pneumatic motors.

Important for the function of a robotic arm is its end effector, which is defined as any equipment mounted on the end of the robotic arm which enables it to interact and manipulate objects and/or the environment [57]. Examples of end effectors may be a simple rigid point used to perform tracking and interaction tasks as seen in [71] or more complex foam extrusion tools for aerial repair as seen in [16].

To understand how robotic manipulators move their end effector the kinematics need to be studied. Kinematics is the study of the movement of bodies or systems without taking into account the forces and torques generating them [11]. Therefore, robotic kinematics describes the position and orientation, also known as pose and their derivatives of all the bodies that make the robotic mechanism.

Important elements of a kinematic analysis are the forward and inverse kinematics of the robotic manipulator along with the workspace and singularities. These terms are further elaborated in the following subsections.

3.1.1. Forward Kinematics

By forward kinematics, we refer to the problem of finding the position and velocity of the end effector, relative to the base, from the positions of all the joints and the geometry of the rigid bodies connecting them [11].

The forward kinematics problem is typically solved by calculating the transformation matrix between a coordinate system defined at the end effector and the coordinate system defined at the base of the robotic manipulator. For serial-chain manipulators, this is often done by computing and concatenating individual transformations between coordinate systems defined at each joint of the manipulator. For closed-chain manipulators, the problem is more complex due to additional constraints.

3.1.2. Inverse Kinematics

The inverse kinematic problem is the counterpart of the forward kinematics. Inverse kinematics aims to solve the required joint positions to achieve a specified end effector pose.

For serial-chain manipulators, this problem requires solving a set of non-linear equations. With such non-linear equations, it may be that multiple or no solutions exist. For these to exist the desired position and orientation of the end effector must lie in the achievable workspace. Often these solutions are found through the use of numerical methods.

Contrary to the forward kinematics problem, the inverse kinematics of closed-chain manipulators is more straightforward and in many cases can be found analytically.

3.1.3. Workspace

The workspace in robotic manipulation is defined as the ”total volume swept out by the end-effector as the manipulator executes all possible motions” [11]. This volume of space is determined by the configuration and the joint limits of the robotic manipulator.

Different types of workspaces can be defined, namely dextrous, maximal, and orientation workspaces. The first defines the locations that the end effector can reach in any orientation, the second defines all locations that can be reached with at least one orientation and the last type of workspace encompasses the set of orientations that can be achieved from a given end effector position [11].

Typically, dexterous workspaces exist only for some ideal geometries, therefore in practice, serial-chain robotic manipulators partition their joints into a regional and an orientation structure. Regional structure joints take care of the positioning of the end effector in space whereas orientation structure joints take care of the orientation of the end effector [11]. Thanks to these definitions by integrating through the possible joint movements the regional workspace can be found and the orientation structure is typically given by the centre of rotation of the wrist of the manipulator.

For closed-chain manipulators the workspace is usually more complex to define as the motion capabilities are typically coupled. The workspace for these manipulators is the intersection of the workspaces of the individual supporting chains [11].

Intuitive ways of solving for the workspace of a manipulator can be solving the forward kinematics for end limits of all joints in the manipulator. Furthermore, the inverse can be done by solving the inverse kinematics for a given position and checking whether this is a reachable position [52].

3.1.4. Singularities

The workspace of a robotic manipulator is also limited by singularities. These are configurations ”in which the robot end-effector becomes blocked in certain directions” [55]. Singularities arise when two or more joints become aligned or nearly aligned leading to unstable end-effector movements.

A particular robot configuration is singular when the Jacobian matrix representing it is rank deficient, meaning that in such configuration there are no solutions for the velocities and accelerations in a specific direction. Hence, it is possible to identify the locations of singularities by deriving locations where the determinant of the Jacobian is equal to zero.

Identifying singularities is important as the motion of the robotic manipulator should not enter or pass too near a singular configuration. Hence motion planners for robotic manipulators should take them into account to generate singularity-free motions.

3.2. Manipulator Types

As alluded to in the previous sections robotic manipulators can be differentiated into two categories namely serial-chain or serial manipulators and closed-chain or more commonly referred to as parallel manipulators. Some of their most defining characteristics and differences are briefly described below.

Serial manipulators typically have a large workspace, their end-effector positioning error is the sum of the joint position errors, their mass is distributed along the manipulator and they are typically more compliant.

Parallel manipulators on the other hand have a smaller workspace, their positioning error is the average of the joint position errors, their mass is concentrated at the base and they are typically more rigid.

These types of manipulators are defined and elaborated further in the following subsections.

3.2.1. Serial Manipulators

Serial manipulators are composed of sequencing links and joints in series. Typically such manipulators as previously mentioned separate rotational and regional structures. The first three joints of the manipulator take care of the positioning of the end-effector and the last three handle its orientation.

Examples of serial manipulators are the Da Vinci surgical robot [38] which uses multiple robotic arms equipped with different tools to perform minimally invasive surgery. The serial-chain robotic arms are equipped with a wrist with no singularities which is important during delicate operations such as surgery.

Typically serial manipulators are employed for industrial activities. Examples of this are the SCARA robot which is an industrial robotic manipulator for small robotic assembly [26]. This manipulator has a cylindrical workspace and is mostly used for pick-and-place tasks.

Larger serial manipulators are used in the automotive industry for the production of cars. An example are the KUKA arc welding robots used to automate welding [45]. These are large, expensive, and stiffer systems which can achieve high precision and accuracy efficiently.

Serial manipulators are effective in industrial applications as they can have a large workspace and achieve accurate positioning through the use of stiff materials and expensive and accurate actuators. Although these manipulators have been used in aerial manipulation systems, such as in the work of Cataldi et al. [15], they introduce several challenges. As the weight of the manipulator is spread along the manipulator and not the base this induces stability issues and strong coupling effects between the manipulator and aerial platform. This leads to more complicated controllers which take into account the full dynamic model of the aerial manipulation system as done in this paper.

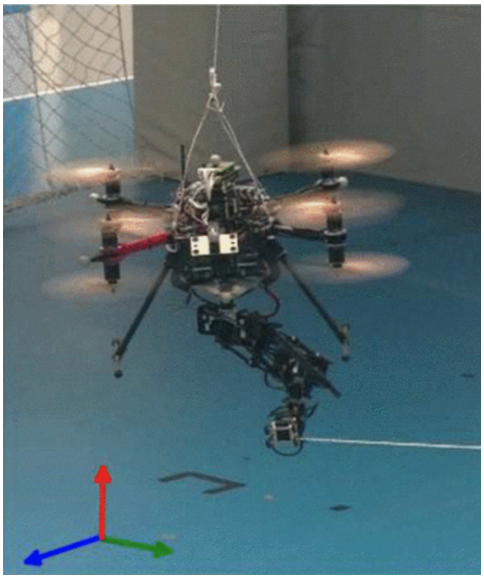

Figure 3.1: Serial manipulator by Cataldi et al.[15].

An attempt to solve such challenges was performed by Suarez et al. [77] by designing a lightweight and compliant arm in order to reduce the coupling effects between the manipulator and aerial platform through weight reductions of the manipulator.

Furthermore, as the positioning error of a serial manipulator is the sum of the errors of all the joints, accurate positioning through inverse kinematics can only be achieved through the use of heavy and precise servo motors at the joints of the manipulator. This further leads to an unfavourable mass distribution.

The work of Imanberdiyev et al. [37] attempted to solve this issue by developing a lightweight dual-arm manipulator. The actuators of the arms are placed near the base of the manipulator and the joints are actuated through the use of transmission systems. This improves the weight distribution of the manipulator.

Numerous works have also employed serial manipulators for their large workspace and their considerable reach capabilities. An example is the work of Danko et al. [21] where a hyper-redundant manipulator was developed with redundant degrees of freedom. This work showcased that its redundancy could reduce negative impacts on the aerial platform's stability and result in a highly reachable workspace.

3.2.2. Parallel Manipulators

Parallel manipulators are achieved by combining two or more serial chain manipulators at the end-effector, hence their name closed-chain manipulators. Each chain that makes a parallel manipulator may have six DoFs, however, typically only six joints may be actuated out of all joints in the system.

As previously discussed, the workspace of an individual serial chain may be geometrically defined but for a closed-chain manipulator, the workspace encompasses the set of solutions that satisfies all serial chains together. This leads to a more complex solution to the workspace problem and often to a smaller workspace for this type of manipulator.

Parallel manipulators are also employed in industrial applications such as manufacturing and assembly. An example is the Adept Quattro [64] which is a four-axis parallel manipulator that can achieve high speeds and precision typically used for assembly applications.

Contrary to serial manipulators this type of manipulator has its actuators closer to its base. This creates a more favourable mass distribution as the movement of the end effector has less of an influence on the base. An example is the FLSUN SR 3D printer [27] which is a Fused Deposition Modelling (FDM) printer which uses a parallel manipulator to extrude material. Thanks to its design it is one of the fastest commercially available FDM printers.

Furthermore, parallel manipulators can also be used for more load-intensive applications such as flight simulators. The closed-loop kinematic chain which defines parallel manipulators leads to high load-carrying capacity while achieving good positioning accuracy. An example is the CAE 7000XR [13], which is a full-flight simulator which is recognized as the ”gold standard” for the high fidelity and reliability it is capable of achieving.

Being closed chain systems makes finding the arbitrary set of DoFs describing parallel manipulators hard to describe. This is because the DoFs are dependent on all actuators of the different serial chains composing it leading to a highly coupled system. Therefore, few well-studied configurations exist. These are the Gough-Stewart platform, five-bar linkage and delta robot.

Gough-Stewart platform

The Gough-Stewart platform is a parallel manipulator typically composed of six limbs connecting the base to the end effector. Each limb is made of a spherical, prismatic and universal joint. This manipulator is actuated through the prismatic joint by linear actuators. This configuration allows for six-DoFs and is characterized by its high load capacity, and low positioning error but a small workspace.

Five-bar linkage

Contrary to the Gough-Stewart platform the five-bar linkage uses only revolute joints, of which the two adjacent to the base are actuated by servo motors. This type of parallel manipulator is composed of five links and five joints, one link serves as the base and the revolute joints attached to it are actuated to control the two-dimensional position of the end-effector.

Delta robot

The Delta robot has similar mechanics to the five-bar linkage with the addition of a third limb which enables motion in three dimensions. The limbs of the Delta robot are composed of an actuated revolute joint at the base, two links connected through spherical joints, and a universal joint connecting to the end effector. The mass distribution of this configuration is concentrated at the base leading to fast movements of the end effector. On the other hand, this type of parallel robot has a lower load capacity compared to other configurations and has singularities present in the workspace.

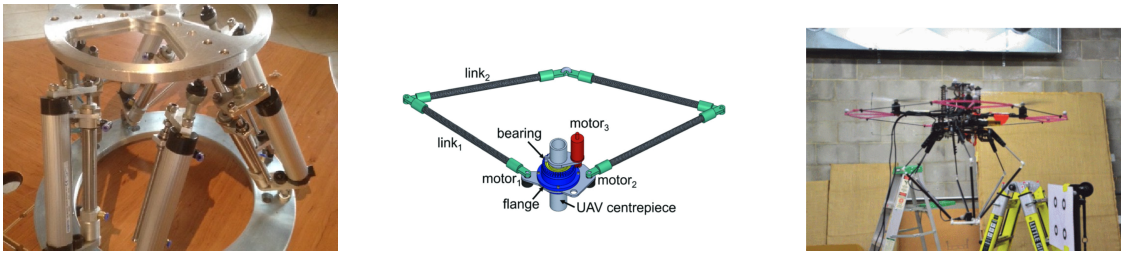

Figure 3.2: Gough-Stewart platform [6] (left) Five-bar linkage[36] (centre), Delta robot [20] (right).

Parallel manipulators are often used in aerial manipulation, in fact as introduced in Section 2.1.2 amongst the first generation of aerial manipulators Fumagalli et al. [30] developed an aerial manipulator equipped with a parallel manipulator with a three DoF delta structure. The delta manipulator was equipped with a three-passive-DoF end effector which allowed for a more compliant behaviour during interaction with the environment.

Another example of a delta manipulator used in aerial manipulation is the work of Danko et al. [20] where they presented an aerial manipulator with a larger delta manipulator on a quadrotor. Their work showcased that the faster dynamics of this parallel manipulator were able to compensate for imprecision in the aerial platform's positioning and improve disturbance rejection with respect to end-effector positioning.

Hamaza et al. [36] showcased the design of an aerial manipulator using a five-bar linkage mechanism for accurate aerial interaction tasks over curved surfaces. By mounting the five-bar linkage mechanism to a rotational flange mounted at the body of the aerial platform, an omnidirectional workspace was achieved. This innovative design increases the size of the workspace which is typically limited for parallel manipulator configurations.

3.3. Force Balanced Manipulators

When robotic manipulators move their end-effector they introduce forces and moments on their base. In the case of aerial manipulation, these effects on the base introduce disturbances and stability issues on the aerial platform carrying the robotic manipulator. Often this results in a highly coupled system which may lead to the design of complex controllers to control them.

Force balanced manipulators are a class of manipulators which aim to eliminate or reduce the reaction forces generated by their movement. This class of manipulators is attractive for aerial manipulation purposes as it is often desired to eliminate or reduce coupling effects between the robotic manipulator and aerial platform.

Three different definitions of balancing exist namely, static, force and dynamic balancing. Static balancing occurs when a system counters the forces of gravity and remains stable in any configuration, hence the system's potential energy is zero. Force balancing instead entails that the net forces acting on the base of the system are zero. Finally, Dynamic balancing occurs when both the net forces and moments acting on the base are zero. Therefore, a dynamically balanced system is a force-balanced system and a force-balanced system is also a statically balanced system. However, the opposite may not be true.

The following subsections will further elaborate on mechanisms which can achieve force and dynamic balancing and applications of force balancing in aerial manipulation.

3.3.1. Force Balancing Mechanisms

Force and dynamic balancing can be achieved in two ways, balancing prior to the kinetic synthesis and balancing after the design.

With regards to balancing after the design this often entails the addition of separate counter masses, counter rotations, special combinations of linkages springs and masses, Counter Rotary Counter-Masses (CRCM), or Active Dynamic Balancing Blocks (ADBB). All of these mechanisms render a manipulator design force or dynamically balanced. However, a flaw with this design strategy is that they

often add more weight and actuators which make the system much heavier compared to the balancing prior to the kinetic synthesis approach.

An example of a dynamically balanced manipulator after the design is in the work of van der Wijk et al. [83] where they showcased the design of an ADBB unit which balances both the net forces and moments acting on a base. This unit works using a planar 2 RRR manipulator (a similar mechanism to a five-bar linkage) that moves a CRCM. Using the dynamic model of the manipulator to which the ADBU is attached it generates the same forces and moments in the opposite direction to create net force and moment equal to zero.

This design was later attached to a robotic manipulator used for pick and place tasks. The entire system was suspended by cables. The pick and place manipulator moved the end effector around its workspace with the ADBU off and on. Whilst the unit was off the system would oscillate but when the unit was turned on the base would remain almost entirely still.

With prior knowledge of the mass of an object that is picked or a method to measure it during operation the ADBU system is also capable of balancing with variable payloads. This was also showcased performing the same test as previously described while the pick and place manipulator picked up an object.

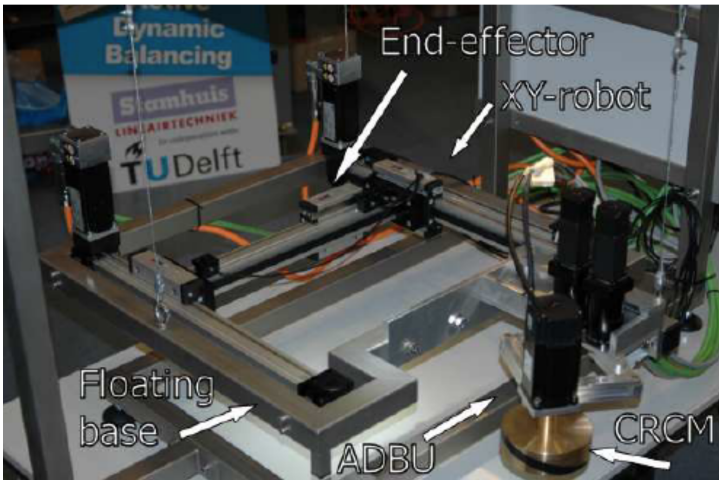

Figure 3.3: Active Dynamic Balancing Unit by van der Wijk et al. [83]

Such balancing systems, as seen through the work of van der Wijk et al., are very effective at rendering net forces and moments equal to zero but come at the expense of having to mount heavy systems. This is acceptable in scenarios where weight is not of concern such as in static robots for industrial applications but it is much less favourable for aerial manipulation. For such an application balancing prior to the kinetic synthesis can yield more suitable designs.

Balancing prior to the kinetic synthesis can be achieved in three different ways, namely, through principal vectors, balanced four-bar mechanisms, and the leg-by-leg approach.

Principal Vectors

Principal vectors or also known as Fisher's method proposes that by adding auxiliary parallelograms to the linkages in a system the centre of mass can be fixed to a determined location [68].

A practical application of this method for robotic manipulation was showcased in the work of van der Wijk [84] where a design for a dynamically balanced delta robot was presented. This was achieved by adding a pantograph mechanism with a counter mass on each limb of the delta robot. The pantograph mechanism settles the centre of mass of the delta robot at a stationary point which leads to a force-balanced system. This however does not result in a moment-balanced system as the angular momentum is dependent on the velocity of the mechanism. Nevertheless, the force-balanced delta robot can be made moment balanced by the introduction of a single actively driven inertia disc.

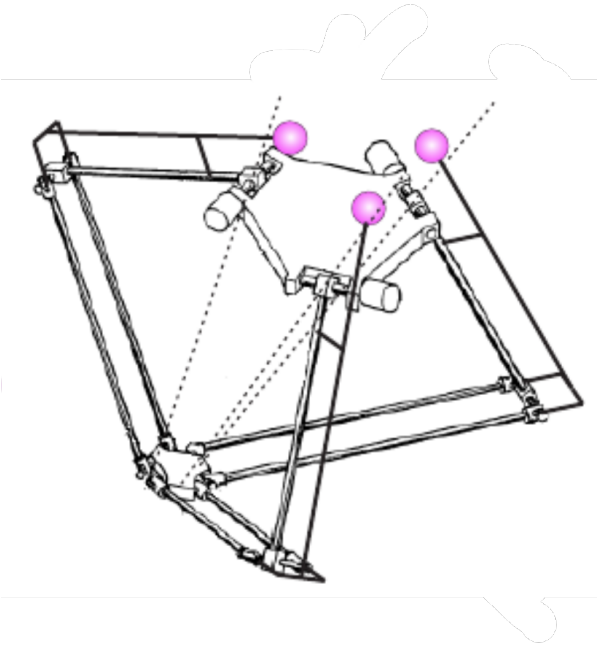

Figure 3.4: Design for force-balanced delta manipulator by van der Wijk et al. [84]

Balanced Four-Bar Mechanisms

Another method to create a dynamically balanced mechanism is by combining balanced four-bar mechanisms. These are similar mechanisms to the five-bar linkage but consist of four links and revolute joints. Furthermore, these are dynamically balanced linkages. As seen in the work of Moore et al. [58] where they determined a set of conditions, derived from solving the kinematics of this mechanism enforcing force and moment balancing constraints, describing balanced four-bar mechanisms.

These planar mechanisms are both force and moment balanced without the use of additional linkages or counterrotations, however, it was found that by combining these planar mechanisms balanced manipulators could be synthesized creating both planar and spatial mechanisms.

An example is the work of Wu [86] where a six DoF parallel mechanism was derived from three 3-DoF parallel mechanisms. Since balanced four-bar linkages are dynamically balanced only in the planar configuration a three-DoF mechanism called the parallelepiped mechanism was designed using three balanced four-bar mechanisms. This was then used as a building block to produce a six DoF dynamic balanced parallel manipulator. The overall system showed to be reactionless at the base but at the cost of a higher degree of complexity. This increased the difficulty to perform the kinematic and dynamic analysis.

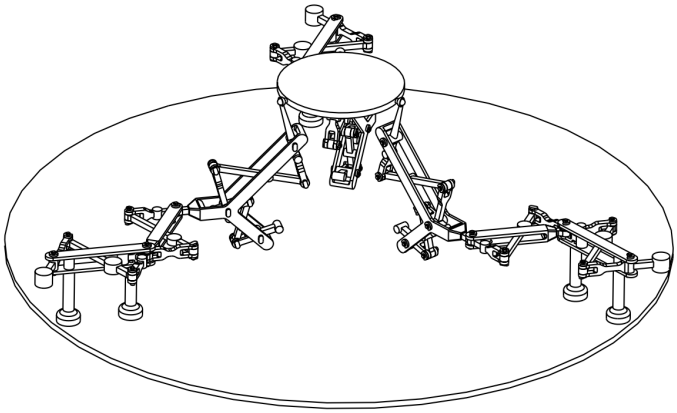

Figure 3.5: Six DoF dynamically balanced manipulator by Wu [86]

Leg by Leg Approach

The leg-by-leg approach follows a similar idea as combining balanced four-bar linkages. In this approach, each leg of a manipulator is dynamically balanced and combined to create a higher DoF dynamically balanced manipulator. This approach however applies to parallel manipulators.

An example of such a system is the PAMINSA robot [10]. This manipulator is composed of pantograph linkages to decouple the vertical and horizontal directions. These are coupled with counter masses to force balance the robot. Moment balancing is instead achieved through motion control of the end effector.

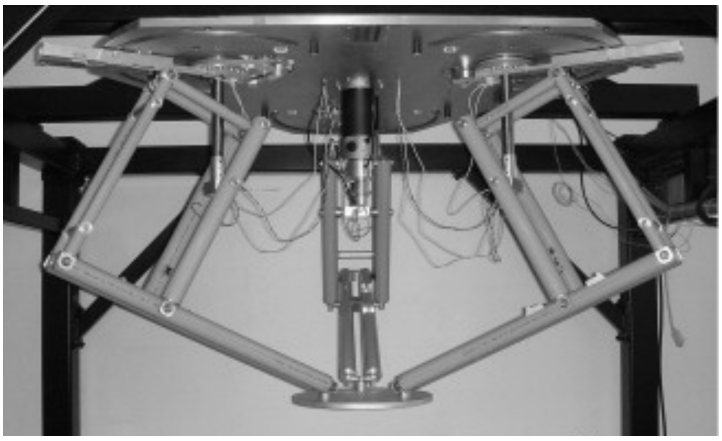

Figure 3.6: PAMISA robot [10]

3.3.2. Force Balancing for Aerial Manipulation

Force-balanced manipulators are attractive mechanisms for aerial manipulation as they limit coupling effects between the manipulator and the aerial platform. This allows for smarter designs which do not rely on complicated control algorithms to counteract such coupling effects. However, the designs implementing this principle are still not vastly adopted in the field of aerial manipulation.

Amongst the first works to address force balancing is the work of Abuzayed et al. [2] where a design for a lightweight aerial manipulator with a Centre of Gravity (CoG) compensation mechanism. A CoG compensation mechanism was developed which worked using a pantograph mechanism and a counterweight. This mechanism would actively compensate for CoG offsets induced by motion or payload variation. This was done in order to increase the stability of the aerial platform by reducing the work the controller needed to do to compensate for CoG offsets.

Another early design taking into account similar CoG considerations is the work of Hamaza et al. [36] with the design of the Omnidrone. The Omnidrone is designed using a five-bar linkage on a rotational flange which enables the manipulator to have an omnidirectional workspace. Furthermore, the manipulator is equipped with a counter mass mounted on a linear bearing allowing it to compensate for CoG offsets produced by the movement of the end effector.

CoG compensation was also implemented for serial manipulator configurations on aerial manipulators. An example is the work of AlAkhras et al. [3] where they showcased the design of a CoG compensation mechanism that could be easily integrated on multirotor platforms. They implemented the mechanism including a design with a serial manipulator for construction inspection purposes. They showcased that even using a serial manipulator which, due to an unfavourable mass distribution, introduces strong coupling effects, the CoG offset mechanism could counteract any offset produced.

A recent innovative design was also produced by Imanberdiyev et al. [37] in which a lightweight dual-arm manipulator was mounted on a hexarotor. In this work, the dual arms were mounted on actuated prismatic joints which could independently move the arms forward and backwards. This is a similar approach to the previous work but instead of moving a mass for CoG compensation the arms would move. Furthermore, having two arms means one arm could be mirrored in the opposite direction as the other to limit shaking forces on the base.

The design and development of a force-balanced delta manipulator based on the previously cited work of van der Wijk [84] was performed by Suryavanshi et al. [80] with the development of the ADAPT

manipulator. ADAPT is a three-DoF reconfigurable force-balanced parallel manipulator which removes reaction forces on the base of the manipulator using a delta configuration with pantographs as limbs and counter masses. This work was designed specifically for aerial manipulation applications but was only tested on a floating base.

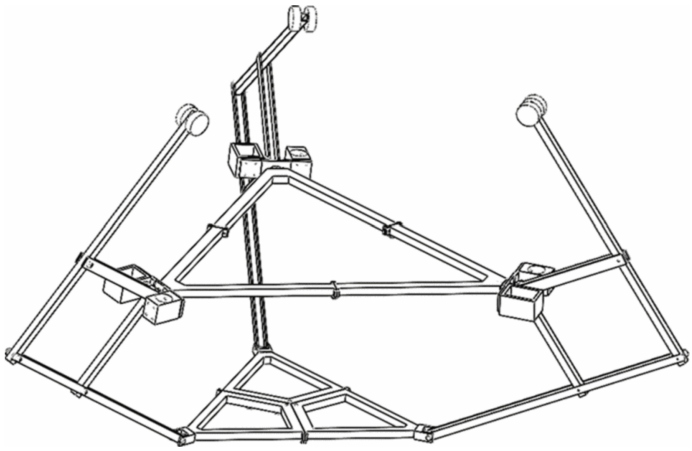

Figure 3.7: ADAPT three-DoF reconfigurable force-balanced parallel manipulator [80]

Clark et al. [17] tested a similar balanced delta robot configuration to Suryavanshi's et al. work on a quadrotor aerial platform. Their work showcased that the balanced manipulator effectively reduced perturbations on the aerial platform but did not show significant improvement in flight accuracy. This was attributed to a large and heavy design of the overall system and a poor integration between the aerial platform and manipulator.

Figure 3.8: Force-balanced delta robot on aerial manipulator by Clark et al. [17]

It is important to note that robotic manipulators such as the ADAPT manipulator [80] or the aerial manipulator presented by Clark et al. [17] remain force balanced only with a fixed payload. Given a variable

payload, the counter masses would need to be reconfigured to achieve a force-balanced mechanism. This issue is not present in aerial manipulators such as the one presented by AlAkhras et al. [3] as the CoG mechanism is independent of the end-effector itself.

Although no practical implementations have been published so far to the best knowledge of the author, articles tackling force-balanced mechanisms for variable payload have been published. An example is from van der Wijk et al. [85] where three approaches to force-balanced reconfiguration were discussed. These were reconfiguration by relocating the balancing mass, reconfiguration by relocating the centre of rotation of the link with balancing mass, and reconfiguration by changing the value of the balancing mass.

It was discussed that the first method would be effective after reconfiguration and lead to less complexity but would not be able to perform the reconfiguration in a force-balanced way. The second method discussed would be able to perform a reconfiguration in a force-balanced manner but would not be able to compensate for drift in the centre of rotation in a force-balanced manner. The final proposed method did not encounter either issue but could produce undesired shaking forces induced by the moving mass.

3.3.3. Payload Estimation

Reconfiguration of force-balanced mechanisms which handle variable payloads requires a fast and accurate estimate of the mass of the payload they manipulate. This section will briefly present methods to estimate the mass of a payload.

Le Rall's work [47] proposed a method to measure the mass of the payload picked up by a robotic manipulator by estimating its inertial parameters. This was done using a Force/Torque sensor and a recursive total least squares algorithm. This method could effectively estimate the mass and inertial properties of the grasped object during the motion of the manipulator. The performance however decreased noticeably during higher-speed operations and short recording times.

Falezza et al. [25] followed a different approach to identify the payload mass of a delta robot. By modifying the model equation of the delta manipulator to account for payload mass, a least square regression algorithm was implemented to estimate the mass from the torque measurements of the actuators. This approach showed satisfactory results but the performance would degrade with larger payloads.

The methods presented show that active reconfiguration of a force-balanced manipulator is possible without prior knowledge of the mass of the object being grasped. However, the performance of such methods should also be tested on a mobile platform.

3.4. Grippers

Thus far only robotic manipulator mechanisms were discussed, so this section will briefly outline tools that are mounted on the robotic manipulator's end effector, specifically, grippers typically used for pick and place tasks.

Pick and place tasks are common in industrial applications and many different types of grippers are used to interact with objects. The most common types typically used in industrial applications are vacuum grippers, pneumatic grippers, hydraulic grippers, and electric grippers [81].

Vacuum grippers work by creating a pressure difference between atmospheric pressure and a vacuum which allows the gripper to hold and move an object. The vacuum can be generated by an electromechanical pump or compressed air pump.

Pneumatic, hydraulic, and electric grippers instead work by closing and opening fingers or jaws. This method is more similar to a human hand grasping an object. The difference between the three is the method of actuation that closes and opens the fingers. Pneumatic grippers use compressed air while hydraulic grippers provide more gripping power through hydraulic fluids. Electric grippers use electric actuators which produce less gripping force but are much lighter.

For aerial manipulation pick and place typically electric grippers are used as they are lighter and less complex to integrate on an aerial platform compared to other solutions. Furthermore, for research purposes, many works do not focus on maximizing the payload capacity during pick and place tasks therefore electric grippers have sufficient gripping force for their purposes.

Examples of grippers for pick and place tasks in aerial manipulation are the works of Cao et al. [14] and Garimella et al. [31] where both works used an electric gripper to move and grab objects. The first work attached a gripper to a delta manipulator and the second attached the gripper to a serial manipulator.

In addition to electric grippers with jaws, magnetic grippers have also been used in the field of aerial manipulation. These facilitate picking an object without requiring a high degree of precision in end effector positioning. Examples of designs which implemented such grippers are the works of Garimella et al. [32] and Jiménez-Cano et al. [40].

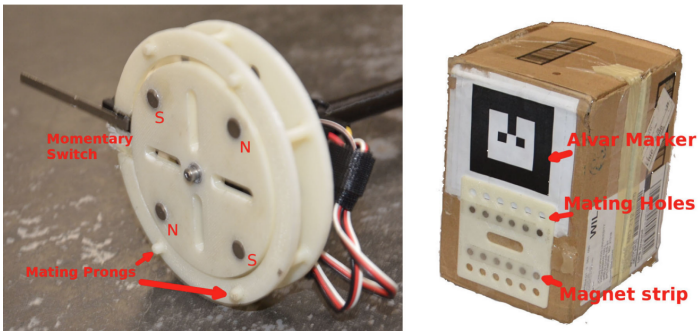

Figure 3.9: Magnetic gripper and object from Garimella et al. [32]

3.5. Research Opportunity

This chapter discussed the working principles of robotic manipulators, two different types of manipulators and force-balanced manipulators which are a promising class of manipulators for aerial manipulation. The aim of this chapter was to define and showcase different robotic arms which are typically used in the field of aerial manipulation and to showcase potential robotic designs which would benefit aerial manipulation applications.

The second sub-question presented in Section 1.1 asked: What type of manipulator morphologies would limit the effect of dynamic end effector movements on its base and how can this be integrated with an aerial platform to achieve a streamlined design? Dynamic end effector movements introduce reaction forces and moments on the aerial platform. However, as discussed in Section 3.3 force balanced robotic manipulators reduce or remove induced reaction forces. This is a favourable property as it reduces the strain on the position controller for the aerial platform and allows for simpler controller designs. Hence, to reduce the effect of dynamic end effector movements force balanced manipulators should be implemented in the aerial manipulator's design.

The cited work of Clark et al. [17] showcased an aerial manipulator design using a force-balanced robotic manipulator. However, the large and poor integration between the manipulator and aerial platform did not show significant improvements in flight accuracy. This indicates that good integration is key to achieving a streamlined design which yields good performance. In order to accomplish this the manipulator base and aerial platform should coincide and an approach similar to the one presented by Suryavanshi et al. [80] should be considered. Finally, a good design philosophy should consider the aerial platform and manipulator as one mechanical entity.

Referring to the third sub-question presented in Section 1.1: "How can state-of-the-art force balancing mechanisms be adapted to tasks with time-varying payloads?" three approaches to handling reconfiguration of a force-balanced mechanism were discussed at the end of Section 3.3.1.

Amongst the three methods reconfiguration by relocating the balancing mass is the most suitable for a force-balanced manipulator such as the design proposed by Suryavanshi et al. [80]. In such a design a linear actuator could move the counter masses on each pantograph leg.

Finally, a research opportunity to design a well-integrated force-balanced manipulator which uses reconfiguration by relocating the balancing masses is available. This design would limit coupling effects between the aerial manipulator and aerial platform and perform dynamic pick and place tasks.

4
Aerial Platforms

UAVs have various different configurations spanning from single-rotor such as helicopters and multirotors which achieve flight solely using their propulsion system to fixed wings which take advantage of the aerodynamic lift generated by the wings, hybrid Vertical Takeoff and Landing (VTOL) platforms or even smaller flapping micro air vehicles. This chapter aims to describe the aerial platforms used for aerial manipulation and their different capabilities.

The outline for this chapter is as follows, Section 4.1 describes the different morphologies for rotor aerial platforms, and Section 4.2 defines the actuation capabilities of such platforms.

4.1. Rotor Platform Types

In aerial manipulation single-rotor or multi-rotor platforms, are mostly used whereas fixed-wing, hybrid VTOL, and flapping-wing aerial vehicles are typically excluded in the selection for a UAM design. This is because these configurations are not as effective in maintaining a fixed position compared to single and multi rotor morphologies. In addition, flapping wings are further constrained from their load payload capacity.
Amongst single and multirotor aerial vehicles different morphologies can be classified. These are helicopters, ducted fans, parallel propellers, tilted propellers, tiltable propellers, multirotor morphing, and multi-platform systems. These are described in the following sections.

4.1.1. Single Rotors

Single rotors encompass configurations such as helicopters. These typically have only one main horizontal rotor or shaft, generating the lift to achieve flight. If necessary in order to counteract the torque from the main rotor a tail rotor, mounted vertically, is used. As described in Chapter 2 these platforms were amongst the first to be used for aerial manipulation, however, in more recent years they have been used less due to their higher mechanical complexity compared to other platforms. Furthermore, helicopters can present a larger risk while flying closer to surfaces.

Examples of helicopters as aerial manipulators are the previously cited works by Bernard et al. [8] and Laiacker et al. [46] where they were used for slung-load transportation and pick and place applications respectively.

Another example of single-rotor configurations are ducted-fans. These consist of a main ducted fan producing lift for flight and other control surfaces which allow it to manoeuvre and stabilize. An example of a ducted-fan used for aerial manipulation was presented in the work of Naldi et al. where the control for a ducted-fan equipped with a parallel delta manipulator was designed for physical interaction tasks[61].

4.1.2. Parallel Multirotors

With parallel multirotors, we define platforms with multiple rotors mounted such that their thrust direction is the same among all of them. Common morphologies for parallel multirotors include quadrotors, hexarotors, and octorotors which have four, six and eight rotors respectively. This category of aerial platform has been commonly used in aerial manipulation due to the low complexity of the system.

Two examples of parallel rotors used for aerial manipulation are the previously cited work of Hamaza et al. where a quadrotor was used for sensor deployment[34] and the work of Suarez et al. who showcased a hexarotor design equipped with a lightweight dual arm manipulator[78].

4.1.3. Tilt Multirotors

Tilt multirotors encompass multirotor designs for which rotors are tilted or are capable of tilting during flight. For these morphologies, the rotors point in different directions which as will later be discussed in Section 4.2 increases the actuation capabilities of the aerial platform.

An example of a tilted rotors aerial manipulator is the previously cited work by Ryll et al. where a hexarotor was used which had all actuators tilted about two axes [71]. This particular multirotor configuration enabled this UAM to perform a peg-in-hole task on a tilted funnel which typically would not have been possible using a parallel multirotor equipped with a rigid end-effector.

For a tilting rotor configuration, Cuniato et al. showcased an aerial manipulator which uses a tricopter frame design with two coaxial rotors which are capable of tilting[18]. This configuration does not have rotors with a fixed tilt but they can adjust their tilt angle.

4.1.4. Morphing Multirotors

Morphing multirotors are aerial platforms with a main body that can reconfigure itself. They can also have tilted or tiltable rotors. These characteristics allow the platform to not only change the direction of thrust of the actuators but also to change the relative position between each actuator. This allows it to better adapt to the environment.

An example of a morphing aerial platform used for aerial manipulation is the work of Zhao et al. who showcased a transformable aerial robot composed of two-dimensional multilinks [87]. The morphology of this platform was taken advantage of to perform whole-body grasping tasks by morphing the body around an object.

4.1.5. Multi-platform systems

This last category of aerial platforms describes vehicles created by physically interlinking multiple rotor platforms such as all of the previously mentioned. The physical interlinking creates a new platform for which the control scheme is different compared to the individual sub-platform and requires the coupling effects between them to be considered for safe flight.

Slung-load transportation by multiple unmanned helicopters is an example of such an aerial configuration. This was showcased in the previously mentioned work by Bernard et al. [8]. A similar example is the work by Sanalitro et al. where the position and orientation of a cable-suspended load are fully controlled by multiple quadrotors[72].

4.2. Actuation Capabilities

The previous section discussed different types of configurations for aerial platforms, however, another way to classify them is by their actuation capabilities. By actuation capabilities, it is inferred the set of feasible wrenches a platform can achieve. For this the allocation matrix, which defines how a variation in inputs affects the total wrench generated by the vehicle, is important. Furthermore, the actuation capabilities are not necessarily dependent on the category of rotorcraft as two different aerial vehicles belonging to the same category as defined in Section 4.1 may have different actuation properties.

4.2.1. Uni-directional Thrust

Uni-directional thrust platforms are capable of generating thrust only in one direction. This allows the platform to produce a force in the vertical direction and torques in all directions. This entails that the allocation matrix has rank four.

Aerial platforms in this category are single rotors or parallel multirotors as for both these vehicle configurations the actuators that generate the lift required for flight are pointing in the same direction. Aerial vehicles with unidirectional thrust capabilities encompass a vast majority of commercial UAVs and are frequently used for aerial manipulators. Examples of such aerial manipulators can be found in Section 4.1.1 and Section 4.1.2.

4.2.2. Multi-directional Thrust

Multi-directional thrust platforms instead are capable of generating thrust in multiple directions. Hence, such aerial platforms have an allocation matrix with rank between five and six. Within this category three more definitions can be made namely fully actuated, over actuated, and omnidirectional platforms. These are defined below.

Fully Actuated

Fully actuated platforms have an allocation matrix with a rank of six. This means that the thrust can be varied in all directions independently from the generated moment. This allows for more control over the position and orientation of the vehicle which is ideal for some aerial manipulation tasks as seen in the previously mentioned work by Ryll et al. which showcased a fully actuated hexarotor[71]. The hexarotor being fully actuated is what enabled the UAM to perform the peg-in-hole task on a tilted funnel using a rigid end-effector.

Over Actuated

Over actuated platforms are fully actuated platforms which have more actuation inputs than DoFs. This means that for a given wrench there is more than one combination of inputs which can realize it. An example of an over actuated platform is the work of Watson et al. where they presented an aerial manipulator using a tricopter configuration with two main thrusters capable of thrust vectoring around two axes[82].

Omnidirectional

Omnidirectional platforms are capable of moving in any direction from almost any orientation. This category is not exclusive from over actuated platforms, in fact, the aerial manipulator mentioned to be over actuated is also omnidirectional. Another example of an omnidirectional aerial platform is the work by Allenspach et al. showcasing a tilt-rotor micro air vehicle with omnidirectional capabilities[5].

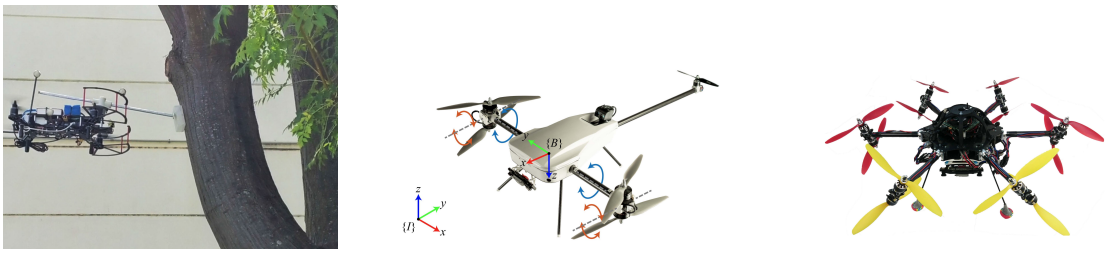

Figure 4.1: Under-actuated parallel multirotor aerial platform [34] (left) Over actuated tiltable rotors aerial platform [82] (centre), Omnidirectional tiltable rotors aerial platform [5] (right).

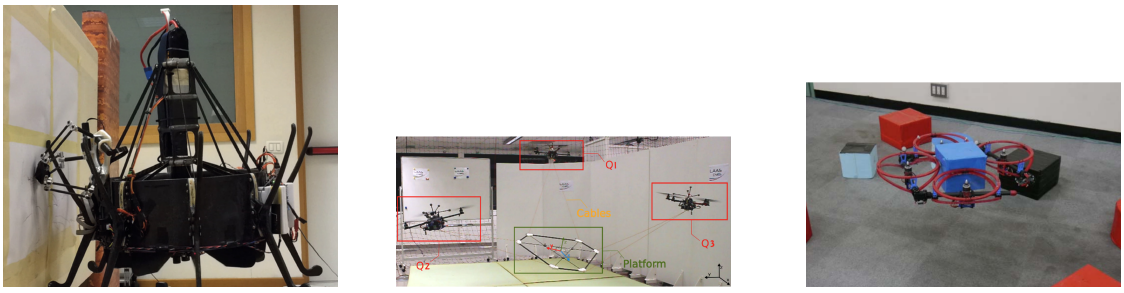

Figure 4.2: Under-actuated ducted fan aerial platform [61] (left) Multiplatform aerial system [72] (centre), Under actuated morphing aerial platform [87] (right).

4.3. Research Opportunity

This chapter discussed different rotor platforms commonly used in the field of aerial manipulation and their actuation capabilities. The aim of this chapter was to showcase these different aerial platform morphologies to determine a suitable match for a well-integrated aerial manipulator design which should perform dynamic pick and place tasks using an active force-balanced manipulator.

Recent research of aerial manipulators focuses on complex aerial platform morphologies using multi-direction thrust actuation properties to develop aerial manipulators. However, as the research opportunity thus far is to develop an active force-balanced aerial manipulator, multi-directional thrust platforms would not give an added benefit but instead add unnecessary degrees of complexity for the purpose of this research.

Furthermore, underactuated platforms such as parallel multirotors cannot control translational motion and attitudes independently therefore, they would benefit from a reduction in coupling effects generated by a robotic manipulator.

Hence, answering the fourth sub-question presented in Section 1.1: What type of aerial platform would benefit the most from an active force balancing system, eg. quadrotor, tiltrotor etc.? An under-actuated parallel multirotor would benefit the most from an active force balancing system.

5
Aerial Manipulation Control

Control in aerial manipulation requires the control of aerial platform and the robotic manipulator attached to it. Two main approaches can be taken, namely, centralised and decentralised control. The first regards the two systems as separate whereas the second considers them as one. This distinction yields very different controller architectures as will be discussed below.

This chapter will discuss centralised control and decentralised control in Section 5.1 and Section 5.2 respectively. Section 5.3 will dive deeper into position controllers for aerial platforms.

5.1. Centralised Control

Centralised control also known as coupled control treats the aerial platform and robotic manipulator as a coupled system. This requires the full dynamic model of the coupled system. This entails that the resulting forces and moments introduced by the movement of the robotic manipulator are modelled within the system.

An example of an aerial manipulator controlled with a centralised approach is the work of Kim et al. [42] where they designed an aerial manipulator using a quadrotor with a two DoF robotic arm. The controller was developed considering the quadrotor and the robotic arm as a combined system. The coupled kinematic and dynamic models were derived and an adaptive sliding mode controller was implemented.

The kinematic model derived included the positions of the quadrotor in the inertial frame, the Euler angles of the quadrotor and the joint angles of the robotic manipulator. To derive the dynamic model the Lagrange-D'Alembert equation was used. Finally, an adaptive sliding mode controller was implemented. This is a type of nonlinear control algorithm which alters the dynamics of the system by applying a discontinuous control signal. This allows it to be more robust to disturbances.

Furthermore, an adaptive controller was implemented as the aerial manipulator was designed for pick and place tasks. Accurate position hold was required for accurate manipulation hence an adaptive controller was desired in order to handle disturbances derived by the additional torques generated by picking up an object.

Results showcased that even without prior knowledge of the mass or inertia of the object being picked up the controller was sufficiently robust to these perturbations leading to a root-mean-squared error in the position hold of the quadrotor of only 2.56 cm.

Another example of a centralised control approach is the work of Cataldi et al. [15] who developed an impedance controller for an aerial manipulator. Their controller was tested on a quadrotor aerial platform with coaxial motors and a six DoF serial manipulator. An impedance controller aims to control the relationship between motion and force and it is typically employed for interaction tasks. An impedance controller can lead to more compliant behaviour with the environment.

Similarly to the previous work the position, orientation of both the aerial platform and end-effector are considered in the kinematic and dynamic model of the coupled system. The proposed controller is composed of three modules, namely, an impedance module, an inverse kinematic module, and a motion controller.

The impedance module filters a desired trajectory, generated by an offline planer, in order to achieve a compliant behaviour. The second module generates the required control inputs for the coupled model, and finally, the third module ensures correct motion tracking.

Their work showcased that compliant behaviour was achievable and that the interaction forces with the environment could be effectively absorbed by the manipulator. Furthermore, when compared to a rigid

controller the impedance controller could handle disturbances which would lead the rigid controller to instability.

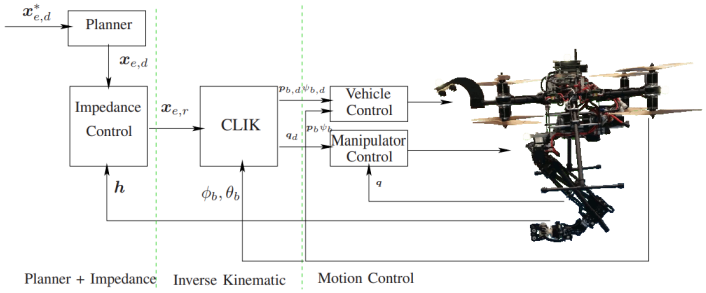

Figure 5.1: Example of a centralised control architecture from Cataldi et al. [15]

Another example of a centralised control approach for a pick and place aerial manipulator is the work of Garimella et al. [31]. Similarly to the work of Kim et al. [42], a quadrotor with a two DoF manipulator was used and the coupled kinematic and dynamic model was used.

This work however implemented a nonlinear model-predictive controller. This type of control algorithm uses a process model to predict the future behaviour of the system. The implemented model predictive controller generates optimal reference trajectories and as it cannot run online in real time it is coupled with a high-frequency low-level controller which tracks the generated reference trajectories.

This controller was tested against a simpler PID controller which was outperformed as the model predictive controller could perform the retrieval task much faster than the PID controller. This was attributed to the fact that the simpler controller did not take into account the dynamics of the arm which would lead to non-smooth end effector positioning which would take longer to converge to the grasping location.

The examples presented showcased good performance however they came at the cost of complex kinematic and dynamic modelling and elaborate control architectures. As seen in the work of Garimella et al. [31] the model predictive controller which relies on solving an optimisation problem could not be used for real-time control due to computational limitations. Although a high performance can be achieved through centralised control architectures this may also come at a high cost, especially for aerial manipulators with a high degree of complexity.

5.2. Decentralised Control

Decentralised control also known as decoupled control treats the aerial platform and robotic manipulator as a decoupled system. This means that the robotic manipulator and aerial platform are seen as separate entities and each is controlled individually. Hence, the resulting forces and moments generated by the manipulator's motion are treated as disturbances by the control scheme.

An example of an aerial manipulator controlled through a decentralised is the work of Zhang et al. [16] where they showcased a design for aerial repair. The controller developed considered the delta robot manipulator and quadrotor platform as decoupled systems. Therefore, different controllers were implemented for each.

The aerial platform controller was a model predictive controller which enabled high-precision position control. Multi-sensor fusion was also implemented for the state estimation of the platform pose. Furthermore, their design could work with a motion capture system and VI odometry. When using VI odometry, a vision-based positioning technique, a marker system called ARTag was also used to reduce inertial frame shifts over time.

The delta manipulator uses an inverse kinematics controller which uses the inverse kinematic model to command actuator inputs to achieve the desired end effector position. Furthermore, as the delta manipulator has higher dynamics than the aerial platform it also corrects for UAV fluctuations.

As the aerial platform's position and orientation will suffer from fluctuations from the optimal desired trajectory, a compensation approach was implemented. This works by computing the offset in position and orientation between the true and desired UAV positions. A new vector between the true position

and target location is generated and the delta manipulator uses this as the input to the inverse kinematic controller.

This design was tested in multiple realistic tests and the performance was evaluated. It was seen that the random mean square error of the end-effector positioning was at most 2.28 mm for hovering tasks. This test was also repeated with 1 m/s wind which showcased a small increase to a random mean square error of 5.19 mm. Furthermore, the delta manipulator with the compensation approach reduced the random mean squared error by at most 81.4% compared to no compensation.

Another example of an aerial manipulator which increases positioning precision by using a parallel manipulator is the work of Danko et al. [20]. The aerial manipulator design uses a six DoF parallel manipulator with six legs and a decentralised control approach. The aerial platform is controlled through a low-level autopilot and the manipulator is controlled through an eye-in-hand image-based visual servoing controller and the inverse kinematic model.

This work also showcased that the positioning precision of the end effector increases compared to the achievable positioning accuracy of an aerial platform with a rigid tool. The higher dynamics of the manipulator and accurate visual servoing control yield a random mean squared error of at most 1.9 cm in still air and 2.9 cm in wind.

Furthermore, the parallel manipulator was compared to a standard six-DoF serial manipulator. It was found that the serial manipulator would need to exert larger torques to achieve the same end effector positioning compared to the parallel manipulator. This introduced larger coupled effects between the manipulator and aerial platform for which the UAV's controller needed to exert greater effort to maintain a stable hover.

Although both the parallel and serial manipulators were able to perform the tested maneuvres and overall improved the positioning accuracy, the configuration of the parallel manipulator was more desired. This was due to the smaller impact induced on the system's CoG. For such a parallel manipulator most of the mass is located near the base of the manipulator so it induces less coupling effects which is a desired property for decentralised controllers.

A more recent application of a decentralised control approach was showcased in the work of Cuniato et al. [19] where they presented a design for an aerial manipulator with an origami delta manipulator. The aerial platform is a tricopter configuration with tiltable coaxial front rotors and a bidirectional rear propeller. The manipulator is an origami delta manipulator optimised for interaction with the environment.

The aerial platform uses a nonlinear geometric tracking controller adapted to the over-actuated platform. The robotic manipulator instead uses an inverse kinematics controller for end effector positioning. Furthermore, this design uses a similar approach as the work from Zhang et al. [16] by taking into account UAV positioning fluctuations. The position input to the inverse kinematics controller is a corrected target position for position and orientation errors of the aerial platform.

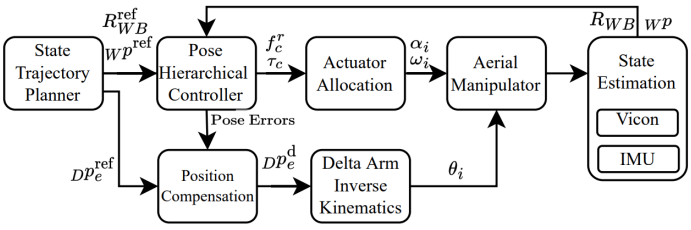

Figure 5.2: Example of a decentralised control architecture from Cuniato et al. [19]

The results from this work also showcased a decrease in position error when using the active delta manipulator. Furthermore, results showcased that a good design with good integration between the aerial platform and robotic manipulator can yield accurate end effector positioning even when treating coupling effects as disturbances.

5.3. Accurate UAV Positioning

Typically Aerial platforms are controlled using simple PID schemes to track a position or velocity error. This approach has worked well for many applications however more complex, model-based, adaptive and nonlinear controllers also exist for improved performance and disturbance rejection. This section will showcase some different controller algorithms developed for multirotor platforms for good disturbance rejection or applied to aerial manipulation.

An example of a PID controller used for aerial manipulation is the work of Orsag et al. [66] where they showcased a cascaded controller with a Proportional controller for the velocity loop and a Proportional Integral controller for the position loop. This particular structure can also be seen as a single PI-D position controller.

Results showcased satisfactory position tracking and stability, furthermore due to the symmetrical design of the three-armed serial manipulator coupling effects did not lead to instability. On the other hand, some oscillations were also present which were not damped out by the controller.

A more complex controller is the backstepping control with sliding mode. This is a powerful nonlinear controller with great stability as it aims to stabilize the whole system through Lyapunov stability theory.

The work of Lee et al. [50] showcased the control of an aerial manipulator using a backstepping controller with sliding mode. They developed the controller for cooperative transportation between aerial manipulators with two DoF robotic arms.

The results obtained showed that even during such a complicated task where the controller needs to handle the additional disturbances introduced by the nature of the cooperative task, the controller achieved satisfactory position and velocity tracking.

Lee et al. [49] also presented a comparison between a classic PID position controller and a backstepping controller with sliding mode. The experiment showcased that in a moderate waypoint tracking task, both controllers achieve satisfactory tracking performances. However, when fast waypoint tracking missions are performed the PID controller behaves worse. This is because PID controllers cannot handle non-linearities and strong disturbances well.

In Section 5.2 a nonlinear model predictive controller implemented by Zhang et al. [16] was introduced. This type of nonlinear controller uses a nonlinear system model to optimize current behaviour based on a prediction of future behaviour. This is achieved through the iterative solution of optimal control problems on a finite prediction horizon.

Another example of a nonlinear model predictive controller is the work of Lunni et al. [53] where they showcased a model predictive controller for the coupled model of the aerial manipulator.

Furthermore, by including all the DoF in the model they implemented an approach to limit CoG shifts in the system. Results showed satisfactory position tracking but slower responses when aligning the robotic arm CoG.

Another nonlinear control algorithm is Incremental Nonlinear Dynamic Inversion (INDI). This control algorithm is more robust than its precursor Nonlinear Dynamic Inversion (NDI) and does not require a full model. These algorithms work by creating a virtual control input from a nonlinear system and using it to control the entire system in a linear way.

Smeur et al. [73] implemented a cascaded INDI controller on a quadrotor aerial platform. The controller uses the INDI algorithm for both attitude control and position control. The results presented showcased this algorithm to be effective and to converge faster than a PID alternative even in windy conditions.

Furthermore, Smeur et al. [74] also worked on an Adaptive INDI algorithm for attitude control which estimates the control effectiveness of the system online. The control effectiveness encompasses values such as a system's inertia and actuator parameters. This is an attractive property for aerial manipulation as the inertia properties change as the robotic manipulator moves.

Nevertheless, INDI to the best knowledge of the author has not been implemented on aerial manipulators. This may be due to not sufficient adaptability during interaction with the environment.

5.4. Research Opportunity

This chapter discussed the two control approaches for aerial manipulators and control algorithms for accurate position tracking of aerial platforms used for aerial manipulation. The aim of this chapter

was to discuss the main control philosophies and determine the most suitable control approach and architecture for a force-balanced aerial manipulator.

As discussed in Section 5.1 centralised controllers consider the aerial manipulator as an individual system. This approach models the coupling effects between the manipulator and aerial platform and leads to good performance but more complex controllers.

By integrating the aerial platform with a force-balanced manipulator the coupling effects between them should be eliminated or reduced by the force-balancing mechanism. Hence, a centralised control approach would be redundant.

Furthermore, with regards to position controllers complex nonlinear control algorithms were presented. The higher degree of complexity of these controllers was often required to compensate for disturbances or to fully control the full model of an aerial manipulator.

Therefore, also in this case implementing a complex position controller with strong disturbance rejection properties would defeat the purpose of integrating a force-balanced manipulator. The simpler PID would provide a better control approach to better showcase the benefits of a smart and well-integrated aerial manipulator design. In addition, the cited INDI-based controllers could also be good position control candidates as they have not yet been proven and tested in the field of aerial manipulation.

To answer the final sub-question presented in Section 1.1: What control approach is best suited for a well-integrated force-balanced aerial manipulator? A decentralised control approach using a simple PID or an unproven INDI position controller is best suited for a well-integrated force-balanced manipulator.

6
Conclusion

This literature review covered the field of aerial manipulation as a whole and the key features of the design of an aerial manipulator, namely the robotic manipulator, the aerial platform and the control architecture. First past and current developments in the field of aerial manipulation were discussed. The different tasks tackled by aerial manipulators were also presented. The working principle and the two types of robotic manipulators, namely serial and parallel manipulators, were then discussed. Force-balanced manipulators were then introduced as an attractive class of robotic mechanisms for aerial manipulation. This was followed by a brief introduction on grippers for pick and place tasks. The different aerial platforms and their actuation properties were showcased next. Then the two different control approaches used in aerial manipulation, namely centralised and decentralised control, were presented. Finally, different position control algorithms were discussed.

This thesis project aims to develop a well-integrated design for an aerial manipulator which limits the induced forces and moments generated by manipulator movements and is capable of performing fast dynamic pick-and-place tasks. After performing extensive research no other aerial manipulation system was found implementing a mechanism to counteract coupling effects during variable payload tasks. Furthermore, no research was found on dynamic pick-and-place tasks where the object to be grasped and placed was not static prior to manipulation. From this research gap, the following research question was formulated: **How can a smart mechanical design limit coupling effects between the individual subsystems of an aerial manipulator and be paired with a control scheme to perform dynamic pick-and-place tasks requiring fast manipulator movements?**. In order to tackle this research question the problem was split between the robotic arm mechanical design, the aerial platform configuration, and the control approach.

In order to limit coupling effects induced by the end effector a force-balanced manipulator can be used, specifically a force-balanced delta parallel manipulator. By using such a robotic manipulator the strain on the flight controller of the aerial platform is reduced. Furthermore, in order to maintain the force-balanced properties during variable payload tasks reconfiguration by relocating the balancing masses can be implemented using linear actuators to shift the counter masses.

In order to highlight the influence of the active force-balanced manipulator and to produce a well-integrated with a low degree of complexity aerial manipulator an under-actuated parallel multirotor aerial platform will be used in the design.

The aim of this project is to develop a design which creates a well-integrated system which does not require complex systems with many degrees of freedom to obtain good performances. Furthermore, a smart design should lead to a less complex controller architecture. In order to accomplish this a good design philosophy should consider the aerial platform and manipulator as one mechanical entity. This approach ensures that the desirable properties from each subsystem can cohesively create a system which performs equivalent to more complex designs.

Finally, a decentralised control approach will be used. Since the coupling effects between the robotic manipulator and aerial platform are limited by the force-balancing mechanism a centralised controller would be redundant as the main idea behind this type of controller is to model the entire system which includes these coupling effects. Therefore, the robotic manipulator will be controlled using an inverse kinematics controller and the aerial platform will use a position controller. The position controller, for the same reason why a centralised control architecture is not used, should have a simple architecture such as a PID controller or should be a novel algorithm which has not been implemented on aerial manipulators such as INDI.

In conclusion, a novel aerial manipulation design will be developed using a parallel multirotor aerial platform and an active force-balancing delta manipulator. The design will follow a smart design approach

for a well-integrated system which will be tested on a dynamic pick-and-place task.

Bibliography

[1] Hani Abu-Jurji and S Hamaza. “Sensorless Impedance Control for Curved Surface Inspections Using the Omni-Drone Aerial Manipulator”. MA thesis. Delft University of Technology, 2022.

[2] Ibrahim Abuzayed, Abdul Rahman Itani, Aser Ahmed, Mohammad Alkharaz, Mohammad A. Jaradat, and Lotfi Romdhane. “Design of Lightweight Aerial Manipulator with a CoG Compensation Mechanism”. In: *2020 Advances in Science and Engineering Technology International Conferences (ASET)*. 2020, pp. 1–5. DOI: 10.1109/ASET48392.2020.9118288.

[3] Ayham AlAkhras, Ilham Hassan Sattar, Muhammad Alvi, Mohammed W. Qanbar, Mohammad A. Jaradat, and Muhannad Alkaddour. “The Design of a Lightweight Cable Aerial Manipulator with a CoG Compensation Mechanism for Construction Inspection Purposes”. In: *Applied Sciences* 12.3 (2022). ISSN: 2076-3417. DOI: 10.3390/app12031173. URL: https://www.mdpi.com/2076-3417/12/3/1173.

[4] Albert Albers, Simon Trautmann, Thomas Howard, Trong Anh Nguyen, Markus Frietsch, and Christian Sauter. “Semi-autonomous flying robot for physical interaction with environment”. In: *2010 IEEE Conference on Robotics, Automation and Mechatronics*. 2010, pp. 441–446. DOI: 10.1109/RAMECH.2010.5513152.

[5] Mike Allenspach, Karen Bodie, Maximilian Brunner, Luca Rinsoz, Zachary Taylor, Mina Kamel, Roland Siegwart, and Juan Nieto. “Design and optimal control of a tiltrotor micro-aerial vehicle for efficient omnidirectional flight”. In: *The International Journal of Robotics Research* 39.10-11 (Aug. 2020), pp. 1305–1325. DOI: 10.1177/0278364920943654. URL: https://doi.org/10.1177%2F0278364920943654.

[6] Amir Yazdani. *A Pneumatic 6-DOF Gough-Stewart Robot*. 2012. URL: https://amir-yazdani.github.io/project/stewart/ (visited on 05/26/2023).

[7] W. A. Atherton. “Miniaturization of Electronics”. In: *From Compass to Computer: A History of Electrical and Electronics Engineering*. London: Macmillan Education UK, 1984, pp. 237–267. ISBN: 978-1-349-17365-5. DOI: 10.1007/978-1-349-17365-5_10. URL: https://doi.org/10.1007/978-1-349-17365-5_10.

[8] Markus Bernard and Konstantin Kondak. “Generic slung load transportation system using small size helicopters”. In: *2009 IEEE International Conference on Robotics and Automation*. 2009, pp. 3258–3264. DOI: 10.1109/ROBOT.2009.5152382.

[9] Markus Bernard, Konstantin Kondak, Ivan Maza, and Anibal Ollero. “Autonomous transportation and deployment with aerial robots for search and rescue missions”. In: *Journal of Field Robotics* 28.6 (2011), pp. 914–931. DOI: https://doi.org/10.1002/rob.20401. eprint: https://onlinelibrary.wiley.com/doi/pdf/10.1002/rob.20401. URL: https://onlinelibrary.wiley.com/doi/abs/10.1002/rob.20401.

[10] Sébastien Briot, Vigen Arakelian, and Sylvain Guégan. “PAMINSA: A new family of partially decoupled parallel manipulators”. In: *Mechanism and Machine Theory* 44.2 (2009), pp. 425–444. ISSN: 0094-114X. DOI: https://doi.org/10.1016/j.mechmachtheory.2008.03.003. URL: https://www.sciencedirect.com/science/article/pii/S0094114X08000542.

[11] Siciliano Bruno and Khatib Oussama. *Springer Handbook of Robotics*. Springer, 2016.

[12] Burbank Police. *Drone Program*. 2019. URL: https://www.burbankpd.org/programs/drone/ (visited on 05/26/2023).

[13] CAE. *CAE 7000XR Series Level D Full-flight Simulator*. 2023. URL: https://www.cae.com/civil-aviation/aviation-simulation-equipment/training-equipment/full-flight-simulators/cae7000xr/ (visited on 06/03/2023).

[14] Huazi Cao, Jiahao Shen, Cunjia Liu, Bohr Zhu, and Shiyu Zhao. “Motion Planning for Aerial Pick-and-Place based on Geometric Feasibility Constraints”. In: (June 2023).

[15] E. Cataldi, G. Muscio, M. A. Trujillo, Y. Rodriguez, F. Pierri, G. Antonelli, F. Caccavale, A. Viguria, S. Chiaverini, and A. Ollero. “Impedance Control of an aerial-manipulator: Preliminary results”. In: *2016 IEEE/RSJ International Conference on Intelligent Robots and Systems (IROS)*. 2016, pp. 3848–3853. DOI: 10.1109/IROS.2016.7759566.

[16] Pisak Chermprayong, Ketao Zhang, Feng Xiao, and Mirko Kovac. “An Integrated Delta Manipulator for Aerial Repair: A New Aerial Robotic System”. In: *IEEE Robotics & Automation Magazine* 26.1 (2019), pp. 54–66. DOI: 10.1109/MRA.2018.2888911.

[17] Angus B. Clark, Nicholas Baron, Lachlan Orr, Mirko Kovac, and Nicolas Rojas. “On a Balanced Delta Robot for Precise Aerial Manipulation: Implementation, Testing, and Lessons for Future Designs”. In: *2022 IEEE/RSJ International Conference on Intelligent Robots and Systems (IROS)*. 2022, pp. 7359–7366. DOI: 10.1109/IROS47612.2022.9981736.

[18] Eugenio Cuniato, Christian Geckeler, Maximilian Brunner, Dario Strübin, Elia Bähler, Fabian Ospelt, Marco Tognon, Stefano Mintchev, and Roland Siegwart. *Design and Control of a Micro Overactuated Aerial Robot with an Origami Delta Manipulator*. 2023. arXiv: 2305.01961 [cs.RO].

[19] Eugenio Cuniato, Christian Geckeler, Maximilian Brunner, Dario Strübin, Elia Bähler, Fabian Ospelt, Marco Tognon, Stefano Mintchev, and Roland Siegwart. *Design and Control of a Micro Overactuated Aerial Robot with an Origami Delta Manipulator*. 2023. arXiv: 2305.01961 [cs.RO].

[20] Todd W. Danko, Kenneth P. Chaney, and Paul Y. Oh. “A parallel manipulator for mobile manipulating UAVs”. In: *2015 IEEE International Conference on Technologies for Practical Robot Applications (TePRA)*. 2015, pp. 1–6. DOI: 10.1109/TePRA.2015.7219682.

[21] Todd W. Danko and Paul Y. Oh. “A hyper-redundant manipulator for Mobile Manipulating Unmanned Aerial Vehicles”. In: *2013 International Conference on Unmanned Aircraft Systems (ICUAS)*. 2013, pp. 974–981. DOI: 10.1109/ICUAS.2013.6564784.

[22] Dictionary. *UAV*. 2023. URL: https://www.dictionary.com/browse/uav (visited on 05/26/2023).

[23] DJI. *DJI Agriculture - Better Growth, Better Life*. 2023. URL: https://ag.dji.com/ (visited on 05/26/2023).

[24] DJI. *DJI Releases First Count Of Lives Saved By Drones*. 2017. URL: https://www.dji.com/newsroom/news/dji-releases-first-count-of-lives-saved-by-drones (visited on 05/26/2023).

[25] Fabio Falezza, Federico Vesentini, Alessandro Di Flumeri, Luca Leopardi, Gianni Fiori, Gianfrancesco Mistrorigo, and Riccardo Muradore. “Gray-Box Model Identification and Payload Estimation for Delta Robots□□This work was partly supported by the project MIUR “Department of Excellence” 2018-2022.” In: *IFAC-PapersOnLine* 53.2 (2020). 21st IFAC World Congress, pp. 8771–8776. ISSN: 2405-8963. DOI: https://doi.org/10.1016/j.ifacol.2020.12.1378. URL: https://www.sciencedirect.com/science/article/pii/S2405896320317869.

[26] Fanuc. *SCARA Robots*. 2023. URL: https://www.fanuc.eu/be/nl/robots/robot-filter-pagina/scara-series/selection-support (visited on 06/02/2023).

[27] FLSUN. *Super Racer (SR) So fast*. 2023. URL: https://flsun3d.com/products/super-racer-sr (visited on 06/03/2023).

[28] Fly Zipline. *Zipline Instant Delivery & Logistics*. 2023. URL: https://www.flyzipline.com/ (visited on 05/26/2023).

[29] Fortune Business Insights. *Unmanned Aerial Vehichle (UAV) Market Size, Share & COVID-19 Impact Analysis, By Class, By Technology, By System, By Application, and Regional Forecast, 2020-2027*. 2020. URL: https://www.fortunebusinessinsights.com/industry-reports/unmanned-aerial-vehicle-uav-market-101603 (visited on 05/26/2023).

[30] Matteo Fumagalli, Roberto Naldi, Alessandro Macchelli, Francesco Forte, Arvid Q.L. Keemink, Stefano Stramigioli, Raffaella Carloni, and Lorenzo Marconi. “Developing an Aerial Manipulator Prototype: Physical Interaction with the Environment”. In: *IEEE Robotics & Automation Magazine* 21.3 (2014), pp. 41–50. DOI: 10.1109/MRA.2013.2287454.

[31] Gowtham Garimella and Marin Kobilarov. “Towards model-predictive control for aerial pick-and-place”. In: *2015 IEEE International Conference on Robotics and Automation (ICRA)*. 2015, pp. 4692–4697. DOI: 10.1109/ICRA.2015.7139850.

[32] Gowtham Garimella, Matthew Sheckells, Soowon Kim, Gabriel Baraban, and Marin Kobilarov. “Improving the Reliability of Pick-and-Place With Aerial Vehicles Through Fault-Tolerant Software and a Custom Magnetic End-Effector”. In: *IEEE Robotics and Automation Letters* 6.4 (2021), pp. 7501–7508. DOI: 10.1109/LRA.2021.3093864.

[33] Anna Gaszczak, Toby Breckon, and Jiwan Han. “Real-time People and Vehicle Detection from UAV Imagery”. In: *Proc SPIE* 7878 (May 2011). DOI: 10.1117/12.876663.

[34] Salua Hamaza, Ioannis Georgilas, Manuel Fernandez, Pedro Sanchez, Thomas Richardson, Guillermo Heredia, and Anibal Ollero. “Sensor Installation and Retrieval Operations Using an Unmanned Aerial Manipulator”. In: *IEEE Robotics and Automation Letters* 4.3 (2019), pp. 2793–2800. DOI: 10.1109/LRA.2019.2918448.

[35] Salua Hamaza, Ioannis Georgilas, and Thomas Richardson. “2D Contour Following with an Unmanned Aerial Manipulator: Towards Tactile-Based Aerial Navigation”. In: *2019 IEEE/RSJ International Conference on Intelligent Robots and Systems (IROS)*. 2019, pp. 3664–3669. DOI: 10.1109/IROS40897.2019.8968591.

[36] Salua Hamaza and Mirko Kovac. “Omni-Drone: on the Design of a Novel Aerial Manipulator with Omni-directional Workspace”. In: *2020 17th International Conference on Ubiquitous Robots (UR)*. 2020, pp. 153–158. DOI: 10.1109/UR49135.2020.9144837.

[37] Nursultan Imanberdiyev, Sumil Sood, Dogan Kircali, and Erdal Kayacan. “Design, development and experimental validation of a lightweight dual-arm aerial manipulator with a COG balancing mechanism”. In: *Mechatronics* 82 (2022), p. 102719. ISSN: 0957-4158. DOI: https://doi.org/10.1016/j.mechatronics.2021.102719. URL: https://www.sciencedirect.com/science/article/pii/S0957415821001781.

[38] Intuitive. *Da Vinci by Intuitive*. 2023. URL: https://www.intuitive.com/en-us/products-and-services/da-vinci (visited on 06/02/2023).

[39] A.E. Jimenez-Cano, J. Martin, G. Heredia, A. Ollero, and R. Cano. “Control of an aerial robot with multi-link arm for assembly tasks”. In: *2013 IEEE International Conference on Robotics and Automation*. 2013, pp. 4916–4921. DOI: 10.1109/ICRA.2013.6631279.

[40] A. E. Jiménez-Cano, D. Sanalitro, M. Tognon, A. Franchi, and J. Cortés. “Precise Cable-Suspended Pick-and-Place with an Aerial Multi-robot System: A Proof of Concept for Novel Robotics-Based Construction Techniques”. English. In: *Journal of Intelligent and Robotic Systems: Theory and Applications* 105.3 (July 2022). ISSN: 0921-0296. DOI: 10.1007/s10846-022-01668-3.

[41] Suseong Kim, Seungwon Choi, and H. Jin Kim. “Aerial manipulation using a quadrotor with a two DOF robotic arm”. In: *2013 IEEE/RSJ International Conference on Intelligent Robots and Systems*. 2013, pp. 4990–4995. DOI: 10.1109/IROS.2013.6697077.

[42] Suseong Kim, Seungwon Choi, and H. Jin Kim. “Aerial manipulation using a quadrotor with a two DOF robotic arm”. In: *2013 IEEE/RSJ International Conference on Intelligent Robots and Systems*. 2013, pp. 4990–4995. DOI: 10.1109/IROS.2013.6697077.

[43] K. Kondak, F. Huber, M. Schwarzbach, M. Laiacker, D. Sommer, M. Bejar, and A. Ollero. “Aerial manipulation robot composed of an autonomous helicopter and a 7 degrees of freedom industrial manipulator”. In: *2014 IEEE International Conference on Robotics and Automation (ICRA)*. 2014, pp. 2107–2112. DOI: 10.1109/ICRA.2014.6907148.

[44] Cengiz Koparan, Ali Bulent Koc, Charles V. Privette, and Calvin B. Sawyer. “In Situ Water Quality Measurements Using an Unmanned Aerial Vehicle (UAV) System”. In: *Water* 10.3 (2018). ISSN: 2073-4441. DOI: 10.3390/w10030264. URL: https://www.mdpi.com/2073-4441/10/3/264.

[45] KUKA. *KUKA arc welding robots*. 2023. URL: https://www.kuka.com/en-de/industries/metal-industry/arc-welding/kuka-arc-welding-robots (visited on 06/02/2023).

[46] Maximilian Laiacker, Marc Schwarzbach, and Konstantin Kondak. “Automatic aerial retrieval of a mobile robot using optical target tracking and localization”. In: *2015 IEEE Aerospace Conference*. 2015, pp. 1–7. DOI: 10.1109/AERO.2015.7118992.

[47] François Le Rall. “Estimation of the Mass of a Manipulator Payload in Motion by Means of an FT Sensor”. MA thesis. KTH, School of Electrical Engineering and Computer Science (EECS), 2020, p. 77.

[48] Dongjae Lee, Hoseong Seo, Dabin Kim, and H. Jin Kim. *Aerial Manipulation using Model Predictive Control for Opening a Hinged Door*. 2020. arXiv: 2003.08256 [cs.RO].

[49] Hyeonbeom Lee. "Trajectory tracking control of multirotors from modelling to experiments: A survey". In: *International Journal of Control, Automation and Systems* 15 (Dec. 2016). DOI: 10.1007/s12555-015-0289-3.

[50] Hyeonbeom Lee, Hyoin Kim, and H. Jin Kim. "Path planning and control of multiple aerial manipulators for a cooperative transportation". In: *2015 IEEE/RSJ International Conference on Intelligent Robots and Systems (IROS)*. 2015, pp. 2386–2391. DOI: 10.1109/IROS.2015.7353700.

[51] Quentin Lindsey and Daniel Mellinger. "Construction of Cubic Structures with Quadrotor Teams". In: June 2011. DOI: 10.15607/RSS.2011.VII.025.

[52] F.L. Litvin. "Application of theorem of implicit function system existence for analysis and synthesis of linkages". In: *Mechanism and Machine Theory* 15.2 (1980), pp. 115–125. ISSN: 0094-114X. DOI: https://doi.org/10.1016/0094-114X(80)90051-8. URL: https://www.sciencedirect.com/science/article/pii/0094114X80900518.

[53] Dario Lunni, Angel Santamaria-Navarro, Roberto Rossi, Paolo Rocco, Luca Bascetta, and Juan Andrade-Cetto. "Nonlinear model predictive control for aerial manipulation". In: *2017 International Conference on Unmanned Aircraft Systems (ICUAS)*. 2017, pp. 87–93. DOI: 10.1109/ICUAS.2017.7991347.

[54] Ioannis Mademlis, Nikos Nikolaidis, Anastasios Tefas, Ioannis Pitas, Tilman Wagner, and Alberto Messina. "Autonomous UAV Cinematography: A Tutorial and a Formalized Shot-Type Taxonomy". In: *ACM Comput. Surv.* 52.5 (Sept. 2019). ISSN: 0360-0300. DOI: 10.1145/3347713. URL: https://doi.org/10.1145/3347713.

[55] Mecademic. *What are Singularities in a Six-Axis Robot Arm?* 2023. URL: https://www.mecademic.com/academic_articles/singularities-6-axis-robot-arm/ (visited on 05/28/2023).

[56] Daniel Mellinger, Quentin Lindsey, Michael Shomin, and Vijay Kumar. "Design, modeling, estimation and control for aerial grasping and manipulation". In: *2011 IEEE/RSJ International Conference on Intelligent Robots and Systems*. 2011, pp. 2668–2673. DOI: 10.1109/IROS.2011.6094871.

[57] Merriam-Webster. *end effector*. 2023. URL: https://www.merriam-webster.com/dictionary/end%20effector (visited on 06/12/2023).

[58] Brian Moore, Josef Schicho, and Clément M. Gosselin. "Determination of the complete set of shaking force and shaking moment balanced planar four-bar linkages". In: *Mechanism and Machine Theory* 44.7 (2009), pp. 1338–1347. ISSN: 0094-114X. DOI: https://doi.org/10.1016/j.mechmachtheory.2008.10.004. URL: https://www.sciencedirect.com/science/article/pii/S0094114X08002139.

[59] Mordor Intelligence. *UNMANNED AERIAL VEHICLES MARKET SIZE & SHARE ANALYSIS - GROWTH TRENDS & FORECASTS (2023 - 2028)*. 2023. URL: https://www.mordorintelligence.com/industry-reports/uav-market (visited on 05/26/2023).

[60] Kye Morton and Luis Felipe Gonzalez Toro. "Development of a robust framework for an outdoor mobile manipulation UAV". In: *2016 IEEE Aerospace Conference*. 2016, pp. 1–8. DOI: 10.1109/AERO.2016.7500576.

[61] R. Naldi, A. Macchelli, N. Mimmo, and L. Marconi. "Robust Control of an Aerial Manipulator Interacting with the Environment□□This work has been partially supported by the European project AirBorne (ICT 780960)." In: *IFAC-PapersOnLine* 51.13 (2018). 2nd IFAC Conference on Modelling, Identification and Control of Nonlinear Systems MICNON 2018, pp. 537–542. ISSN: 2405-8963. DOI: https://doi.org/10.1016/j.ifacol.2018.07.335. URL: https://www.sciencedirect.com/science/article/pii/S2405896318310905.

[62] Petr Novák, Klaus Müller, K. S. V. Santhanam, and Otto Haas. "Electrochemically Active Polymers for Rechargeable Batteries". In: *Chemical Reviews* 97.1 (1997). PMID: 11848869, pp. 207–282. DOI: 10.1021/cr941181o. eprint: https://doi.org/10.1021/cr941181o. URL: https://doi.org/10.1021/cr941181o.

[63] Anibal Ollero, Marco Tognon, Alejandro Suarez, Dongjun Lee, and Antonio Franchi. “Past, Present, and Future of Aerial Robotic Manipulators”. In: *IEEE Transactions on Robotics* 38.1 (2022), pp. 626–645. DOI: 10.1109/TRO.2021.3084395.

[64] OMRON. *Quattro*. 2023. URL: https://industrial.omron.eu/en/products/quattro (visited on 06/03/2023).

[65] Matko Orsag, Christopher Korpela, Stjepan Bogdan, and Paul Oh. “Valve turning using a dual-arm aerial manipulator”. In: *2014 International Conference on Unmanned Aircraft Systems (ICUAS)*. 2014, pp. 836–841. DOI: 10.1109/ICUAS.2014.6842330.

[66] Matko Orsag, Christopher Korpela, and Paul Oh. “Modeling and Control of MM-UAV: Mobile Manipulating Unmanned Aerial Vehicle”. eng. In: *Journal of intelligent & robotic systems* 69.1-4 (2013), p. 14. ISSN: 0921-0296.

[67] Matko Orsag, Christopher Korpela, Paul Y. Oh, and Stjepan Bogdan. *Aerial manipulation*. Springer, 2018.

[68] Hans Przibram. “Theoretische Grundlage für eine Mechanik der lebenden Körper”. In: *Monatshefte für Mathematik und Physik* 18 (1907), A38–A39. URL: https://api.semanticscholar.org/CorpusID:197663313.

[69] A. Pumarola, Alexander Vakhitov, Antonio Agudo, F. Moreno-Noguer, and A. Sanfeliu. “Relative Localization for Aerial Manipulation with PL-SLAM”. In: *Aerial Robotic Manipulation: Research, Development and Applications*. Ed. by Anibal Ollero and Bruno Siciliano. Cham: Springer International Publishing, 2019, pp. 239–248. ISBN: 978-3-030-12945-3. DOI: 10.1007/978-3-030-12945-3_17. URL: https://doi.org/10.1007/978-3-030-12945-3_17.

[70] Fabio Ruggiero, Vincenzo Lippiello, and Anibal Ollero. “Aerial Manipulation: A Literature Review”. In: *IEEE Robotics and Automation Letters* 3.3 (2018), pp. 1957–1964. DOI: 10.1109/LRA.2018.2808541.

[71] Markus Ryll, Giuseppe Muscio, Francesco Pierri, Elisabetta Cataldi, Gianluca Antonelli, Fabrizio Caccavale, Davide Bicego, and Antonio Franchi. “6D interaction control with aerial robots: The flying end-effector paradigm”. In: *The International Journal of Robotics Research* 38 (June 2019), p. 027836491985669. DOI: 10.1177/0278364919856694.

[72] Dario Sanalitro, Heitor J. Savino, Marco Tognon, Juan Cortés, and Antonio Franchi. “Full-Pose Manipulation Control of a Cable-Suspended Load With Multiple UAVs Under Uncertainties”. In: *IEEE Robotics and Automation Letters* 5.2 (2020), pp. 2185–2191. DOI: 10.1109/LRA.2020.2969930.

[73] E.J.J. Smeur, G.C.H.E. de Croon, and Q. Chu. “Cascaded incremental nonlinear dynamic inversion for MAV disturbance rejection”. In: *Control Engineering Practice* 73 (Apr. 2018), pp. 79–90. DOI: 10.1016/j.conengprac.2018.01.003. URL: https://doi.org/10.1016%2Fj.conengprac.2018.01.003.

[74] Ewoud Smeur, Q.P. Chu, and Guido Croon. “Adaptive Incremental Nonlinear Dynamic Inversion for Attitude Control of Micro Air Vehicles”. In: *Journal of Guidance, Control, and Dynamics* 39 (Dec. 2015), pp. 1–12. DOI: 10.2514/1.G001490.

[75] Kelly Steich, Mina Kamel, Paul Beardsley, Martin K. Obrist, Roland Siegwart, and Thibault Lachat. “Tree cavity inspection using aerial robots”. In: *2016 IEEE/RSJ International Conference on Intelligent Robots and Systems (IROS)*. 2016, pp. 4856–4862. DOI: 10.1109/IROS.2016.7759713.

[76] Alejandro Suarez, Guillermo Heredia, and Anibal Ollero. “Design of an Anthropomorphic, Compliant, and Lightweight Dual Arm for Aerial Manipulation”. In: *IEEE Access* 6 (2018), pp. 29173–29189. DOI: 10.1109/ACCESS.2018.2833160.

[77] Alejandro Suarez, Guillermo Heredia, and Anibal Ollero. “Lightweight compliant arm with compliant finger for aerial manipulation and inspection”. In: *2016 IEEE/RSJ International Conference on Intelligent Robots and Systems (IROS)*. 2016, pp. 4449–4454. DOI: 10.1109/IROS.2016.7759655.

[78] Alejandro Suarez, Antonio Enrique Jimenez-Cano, Victor Manuel Vega, Guillermo Heredia, Angel Rodriguez-Castaño, and Anibal Ollero. “Design of a lightweight dual arm system for aerial manipulation”. In: *Mechatronics* 50 (2018), pp. 30–44. ISSN: 0957-4158. DOI: https://doi.org/10.1016/j.mechatronics.2018.01.005. URL: https://www.sciencedirect.com/science/article/pii/S0957415818300011.

[79] Alejandro Suarez, Fran Real, Víctor M. Vega, Guillermo Heredia, Angel Rodriguez-Castaño, and Anibal Ollero. “Compliant Bimanual Aerial Manipulation: Standard and Long Reach Configurations”. In: *IEEE Access* 8 (2020), pp. 88844–88865. DOI: 10.1109/ACCESS.2020.2993101.

[80] Kartik Suryavanshi, Salua Hamaza, Volkert van der Wijk, and Just Herder. “ADAPT: A 3 Degrees of Freedom Reconfigurable Force Balanced Parallel Manipulator for Aerial Applications”. In: *2023 IEEE International Conference on Robotics and Automation (ICRA)*. 2023, pp. 11936–11942. DOI: 10.1109/ICRA48891.2023.10160451.

[81] Universal Robots. *Types of Grippers Used in Manufacturing | Universal Robots*. 2023. URL: https://www.universal-robots.com/blog/types-of-grippers-used-in-manufacturing/ (visited on 06/06/2023).

[82] Robert Watson, Mina Kamel, Dayi Zhang, Gordon Dobie, Charles MacLeod, S. Gareth Pierce, and Juan Nieto. “Dry Coupled Ultrasonic Non-Destructive Evaluation Using an Over-Actuated Unmanned Aerial Vehicle”. In: *IEEE Transactions on Automation Science and Engineering* 19.4 (2022), pp. 2874–2889. DOI: 10.1109/TASE.2021.3094966.

[83] Volkert van der Wijk and Just Herder. “Active Dynamic Balancing Unit for Controlled Shaking Force and Shaking Moment Balancing”. In: vol. 2. Jan. 2010. DOI: 10.1115/DETC2010-28423.

[84] Volkert van der Wijk and Just Herder. “Dynamic Balancing of Clavel’s Delta Robot”. In: Jan. 2009, pp. 315–322. ISBN: 978-3-642-01946-3. DOI: 10.1007/978-3-642-01947-0_39.

[85] Volkert van der Wijk and Just L. Herder. “Force balancing of variable payload by active force-balanced reconfiguration of the mechanism”. In: *2009 ASME/IFToMM International Conference on Reconfigurable Mechanisms and Robots*. 2009, pp. 323–330.

[86] Yangnian Wu. “Synthesis and Analysis of Reactionless Spatial Parallel Mechanisms”. PhD thesis. Laval University, Apr. 2003.

[87] Moju Zhao, Koji Kawasaki, Xiangyu Chen, Shintaro Noda, Kei Okada, and Masayuki Inaba. “Whole-body aerial manipulation by transformable multirotor with two-dimensional multilinks”. In: *2017 IEEE International Conference on Robotics and Automation (ICRA)*. 2017, pp. 5175–5182. DOI: 10.1109/ICRA.2017.7989606.

Part IV

References

[This page is intentionally left blank]

References

[1] Aude Billard et al. “Trends and challenges in robot manipulation”. In: *Science* 364.6446 (2019), eaat8414.

[2] Melissa Ryan Karl McLetchie. *Ocean Exploration Technology: How Robots Are Uncovering the Mysteries of the Deep*. 2022. URL: `https://oceanexplorer.noaa.gov/explainers/technology.html` (visited on 11/12/2024).

[3] Abdul Kadir Bin Motaleb et al. “Bomb disposal robot”. In: *2016 International Conference on Innovations in Science, Engineering and Technology (ICISET)*. 2016, pp. 1–5.

[4] Mobile Industrial Robots. *Understanding a Mobile Manipulator Robot*. 2024. URL: `https://mobile-industrial-robots.com/blog/understanding-a-mobile-manipulator` (visited on 11/12/2024).

[5] Fabio Ruggiero et al. “Aerial Manipulation: A Literature Review”. In: *IEEE Robotics and Automation Letters* 3.3 (2018), pp. 1957–1964.